On numerical residuals and physical instabilities in incompressible steady-state fluid flow calculations

Vassilios Theofilis

Rohnsterrassen 14, D-37085 Göttingen, Germany.
tel./fax: +49 551 487625

20000628 106

AQF00-09-2886

REPORT DOCUMENTATION PAGE

Form Approved OMB No. 0704-0188

1. AGENCY USE ONLY (Leave blank)	2. REPORT DATE 20-March-2000	3. REPORT TYPE AND DATES COVERED Final Report

4. TITLE AND SUBTITLE

On numerical residuals and physical instabilities in incompressible steady-state fluid flow calculations

5. FUNDING NUMBERS

F61775-99-WE090

6. AUTHOR(S)

Dr. Vassilios Theofilis

7. PERFORMING ORGANIZATION NAME(S) AND ADDRESS(ES)

Vassilios Theofilis
Rohnsterrassen 14
Gottingen D-37085
Germany

8. PERFORMING ORGANIZATION REPORT NUMBER

N/A

9. SPONSORING/MONITORING AGENCY NAME(S) AND ADDRESS(ES)

EOARD
PSC 802 BOX 14
FPO 09499-0200

10. SPONSORING/MONITORING AGENCY REPORT NUMBER

SPC 99-4090

11. SUPPLEMENTARY NOTES

12a. DISTRIBUTION/AVAILABILITY STATEMENT

Approved for public release; distribution is unlimited.

12b. DISTRIBUTION CODE

A

13. ABSTRACT (Maximum 200 words)

This report results from a contract tasking Vassilios Theofilis as follows: The contractor proposes to perform a three-dimensional linear instability analysis of the nonparallel steady compressible two-dimensional basic flow, which develops inside an open cavity of arbitrary aspect ratio driven by a constant free-stream velocity. The objective of the study is to determine the environmental conditions at which the flow becomes unstable to three-dimensional, periodic in the lateral direction, small-amplitude disturbances. Identification of the spatial structure of both stationary and traveling instabilities as well as prediction of the frequencies of the unstable traveling modes is paramount to devising methods for control of these instabilities. The study will be performed along the lines of his analogous work on the classic incompressible lid-driven cavity; initially steady incompressible and compressible basic states will be determined and compared with existing- and independently-performed work-in-progress; subsequently the nonparallel linear instability analysis of this state will be performed.

14. SUBJECT TERMS

EOARD, Modelling & Simulation, Separated Flows, Cavity Acoustics

15. NUMBER OF PAGES

16. PRICE CODE
N/A

17. SECURITY CLASSIFICATION OF REPORT UNCLASSIFIED	18. SECURITY CLASSIFICATION OF THIS PAGE UNCLASSIFIED	19, SECURITY CLASSIFICATION OF ABSTRACT UNCLASSIFIED	20. LIMITATION OF ABSTRACT UL

Our present concern has been with the identification of the origin and classification of the different qualitative forms which the numerically obtained transient solution assumes, when a two-dimensional direct numerical simulation (DNS) of the incompressible continuity and Navier-Stokes equations is performed in order to recover a steady-stade solution of the system of equations governing fluid flow motion. Within the unifying framework of the extension of Tollmien's linear instability theory [25] to nonparallel two-dimensional steady basic states, residuals encountered in the simulation as the latter approaches convergence are either identified as or associated with the least damped of the two-dimensional global linear eigenmodes of the steady-state flow. The inability to converge to a steady-state is shown to be linked with the global linear flow eigenmodes approaching a neutrally stable state and interacting nonlinearly. With the origin of the residuals established, an algorithm is presented which permits recovery of the converged steady-state solution from transient data at substantially less computing effort compared with that necessary for the integration of the system of equations until convergence. Nonparallel linear instability theory of the three-dimensional eigenmodes of the converged two-dimensional steady-state may also be used to quantify the differences between the results of two- and three-dimensional DNS. The classic two-dimensional lid-driven cavity flow is used as a demonstrator of these ideas.

2

CONTENTS

1. INTRODUCTION

A steady-state solution $\bar{q}$ of the two-dimensional incompressible continuity and Navier-Stokes equations which describe flow in a prescribed two-dimensional domain Ω bounded by $\partial\Omega$ is seeked numerically. A plethora of numerical approaches for the accurate and efficient integration of either the steady or the unsteady equations of motion exists (e.g. [9, 26, 30]) so that this problem may be considered solved in principle. However, in performing a time-accurate integration of the equations of motion one observes that, depending on the values of parameters such as the flow Reynolds number, in the limit of large time either a steady-state solution is obtained (e.g. [1]) or unsteady, sometimes periodic, motion sets in (e.g. [13, 11]). The first question arising is what type of physical information is not considered by solving the steady as opposed to the unsteady equations of motion and what is the physical interpretation of the critical conditions beyond which the steady and unsteady formulations deliver different results. Both physical and numerical experience suggest that at low Reynolds numbers the two formulations may be used interchangeably. For example, essentially identical results with those of Ghia *et al.* [27] and Schreiber and Keller [19] have been obtained by a multitude of subsequent investigators who used the time-dependent equations of motion to describe flow in the square lid-driven cavity at Reynolds numbers up to $Re = 10^4$. On the other hand, the question of existence of a steady-state solution delivered by the unsteady version of the equations of motion at $Re = 10^4$ has been recently re-opened [31], while it is well known that Hopf bifurcations exist in both the aspect-ratio two singular lid-driven cavity at $Re < 5000$ [11] and its regularised square counterpart at $Re \approx 10^4$ [10]. Concensus exists that at high Reynolds numbers the unsteady formulation is capable of delivering physics inaccessible to the steady version of the equations of motion; however, the origin of the differences between the results of the two formulations is presently not understood in a satisfactory manner. This is an alternative way of posing

the first question, namely what are the unsteady effects that manifest themselves at high Reynolds numbers.

The next question arises from the very concept of two-dimensionality. The results of numerical solutions of the three-dimensional analoga of the incompressible continuity and Navier-Stokes equations are in most cases in substantial qualitative and quantitative disagreement with their two-dimensional counterparts (e.g. [2, 7]), relegating two-dimensional DNS to the realm of academic interest. Within the scope of two-dimensional solutions being of interest, three-dimensionality of physical space could be addressed by considering the flow to be independent of the third spatial direction. Homogeneity in this third direction could, in turn, be discussed in the context of a three-dimensional simulation, nonperiodic in the same two spatial directions as the two-dimensional one and periodic in the third. Advances in both algorithms and hardware and, not least, a considerable amount of knowledge on the differences between two- and three-dimensional numerical simulation results lead one to employ a DNS algorithm for flow with two nonperiodic and one periodic spatial direction (e.g. [22, 15, 28]) in the founded expectation that a three-dimensional so-called spatial DNS is the only means capable of capturing all physical phenomena at a certain Reynolds number. The second question which may be posed at this point regards the origin of the differences between the results of such two- and three-dimensional direct numerical simulations. Associated, one may ask whether there exists an alternative means to spatial DNS for the description of the origins of the three-dimensional phenomena encountered.

The objective of the present paper is to put both questions within the unified framework of nonparallel linear instability of the steady state $\bar{q}$. With the aid of a well-studied flow example we demonstrate the intimate link between numerical residuals in steady-state fluid flow calculations and linear two-dimensional eigenmodes of the converged steady state $\bar{q}$. In §2 we present theoretical arguments, first analysing the behaviour of numerical

residuals near convergence towards the steady-state solution from a numerical point of view. Subsequently we discuss solutions of the partial derivative eigenvalue problem governing linear instability of nonparallel two-dimensional steady-state flows, which shed light on residuals from a physical viewpoint. With the origin of residuals established from a physical point of view we construct and present an algorithm which permits recovery of the converged steady-state solution from transient results of the time-marching procedure, the latter taken well before convergence. In §3 we present results obtained for the classic square lid-driven cavity flow as a demonstrator of the ideas discussed herein. The link between the results of nonparallel linear instability theory and different types of behaviour of numerical residuals in the DNS is demonstrated in this section and the aforementioned questions are answered. Examples of recovery of the converged steady-state from transient data and assessment of the substantial savings in the computing effort materialised by use of the proposed algorithm are presented in this section. Closing remarks on the far-reaching implications of the present findings are made in §4 and suggestions for the extension of the present analysis to compressible flow and flow with three nonperiodic spatial directions are made in §5.

2. THEORY

2.1. On residuals and the phenomenology of their behaviour

While in an computation based on the steady system of equations governing fluid flow motion residuals are viewed as departure from the steady state which have to be eliminated in an efficient manner by a specific solution algorithm (e.g. multigrid), in a time-accurate integration one may view transients as solutions of the equations of motion and attempt to attach physical significance to characteristic patterns of their behaviour. Here we concentrate on a time-accurate integration of the unsteady equations of motion and monitor the behaviour of residuals, defined as the difference between the transient solution and the

converged steady state, in flow regimes where the latter exists. Physical space is three-dimensional; without loss of generality we may take the Cartesian coordinates x and y to be defined on Ω while z denotes the third spatial coordinate in the direction of Ω. Along the first two coordinates the velocity vector has components u and v, while pressure is denoted by p. The equations of motion are marched in time t until $\mathbf{q} = (u, v, p)^{\mathrm{T}}$, the transient solution, converges to $\bar{\mathbf{q}}$. Assuming that the latter exists and keeping the domain Ω unchanged, the following qualitative observations are made.

First, at any Reynolds number Re at which $\bar{\mathbf{q}}$ exists, close to convergence the residuals decay exponentially in amplitude. Second, refinement of the discretisation of the domain Ω at constant Re results in convergence of the rate at which the residuals decay. Third, the (converged) rate of decay of residuals is a function of the flow Reynolds number; as Re increases residuals decay slower and the associated time of integration of the equations of motion until convergence increases. Fourth, on occasion, the residuals decay at a specific constant rate for a number of decades before this rate of decay changes to a different constant value at which residuals further decay until convergence. Fifth, systematically increasing Re, instead of monotonic convergence of residuals an oscillatory behaviour of $\mathbf{q}$ in the neighbourhood of $\bar{\mathbf{q}}$ is observed. Ultimately, a value of Reynolds number is reached past which no $\bar{\mathbf{q}}$ exists. At first sight the existence of a physical mechanism which unifies such diverse patterns of behaviour of the numerical solution seems unlikely.

2.2. A numerical point of view on the behaviour of residuals near convergence

However, it is straightforward to provide an explanation of the first observation on the behaviour of residuals, which also provides a handle to the link between numerical residuals and physical flow instabilities. We assume that the solution $\mathbf{q}$ is close to converging to the seeked two-dimensional field $\bar{\mathbf{q}} = (\bar{u}, \bar{v}, \bar{p})^{\mathrm{T}}$ such that it may be decomposed into the latter and small two-dimensional residuals $\tilde{\mathbf{q}}_{2\mathrm{D}} = (\tilde{u}_{2\mathrm{D}}, \tilde{v}_{2\mathrm{D}}, \tilde{p}_{2\mathrm{D}})^{\mathrm{T}}$ superimposed upon it,

according to

$$\mathbf{q}(x, y, t) = \bar{\mathbf{q}}(x, y) + \varepsilon\, \tilde{\mathbf{q}}_{2D}(x, y, t), \tag{1}$$

with $\varepsilon \ll 1$. We next substitute the decomposition (1) into the continuity and Navier-Stokes equations and assume that the steady-state solution satisfies the equations of motion at $O(1)$, such that it may be subtracted out of the resulting system at this order. Subsequently, based on the smallness of the amplitude of the residuals, we linearise about $\bar{\mathbf{q}}$ and rearrange the system at $O(\varepsilon)$ such that the vector of residuals represents the unknowns; terms of $O(\varepsilon^2)$ are neglected. Since the coefficients of the resulting linear system of equations for the determination of $\tilde{\mathbf{q}}_{2D}$ at $O(\varepsilon)$ are independent of time t we may introduce an eigenmode decomposition in this coordinate, according to

$$\tilde{\mathbf{q}}_{2D}(x, y, t) = \hat{\mathbf{q}}_{2D}(x, y)\, e^{\sigma t} \tag{2}$$

with $\hat{\mathbf{q}}_{2D} = (\hat{u}_{2D}, \hat{v}_{2D}, \hat{p}_{2D})^{\mathbf{T}}$. The physical significance of the parameter σ will be discussed shortly; from a numerical point of view it represents the rate at which the residuals $\tilde{\mathbf{q}}_{2D}$ decay in the neighbourhood of $\bar{\mathbf{q}}$. For simplicity we present only the real part of the admissible solutions of (2) although it is clear that both $\hat{\mathbf{q}}_{2D}$ and σ may, in general, be complex while $\tilde{\mathbf{q}}_{2D}$ is always real. Convergence of the solution $\mathbf{q}$ towards $\bar{\mathbf{q}}$ may be monitored by reference to either the local behaviour of the solution $\mathbf{q}$ at a position (x_0, y_0) on Ω or by monitoring a suitably defined global criterion such as the energy contained in the residuals $\tilde{\mathbf{q}}_{2D}$; alternatives have been discussed in [24]. Here we follow the first approach and recover the parameter σ by monitoring the solution at two time-levels, $t - \Delta t$ and t, where Δt may but need not be the time-step in the numerical solution algorithm. Combining (1) and (2) it follows that the time-behaviour of the solution may be monitored by

$$\sigma = \ln[\mathbf{q}^t / \mathbf{q}^{t-\Delta t}] / \Delta t \approx d \ln[\mathbf{q}^t] / dt, \tag{3}$$

where

$$\mathbf{q}^t = |\mathbf{q}(x_0, y_0, t) - \bar{\mathbf{q}}(x_0, y_0)|. \tag{4}$$

The approximation in (3) holds as equality in the case of linear dependence of $\ln[\mathbf{q}^t]$ on time t. Decay of residuals is indicated by $\sigma < 0$. The first statement of the present paper is thus in place without reference to a particular flow, through the analytical result that an exponential decay of residuals near convergence should be observed as a consequence of the separability of the linearised system of equations for the determination of residuals in time.

2.3. A physical point of view based on nonparallel linear instability theory

Explanation of the further observations made in § 2.1 requires calling upon an extension of the classic linear instability theory proposed by Tollmien [25], which describes the behaviour of small-amplitude disturbances superimposed upon an one-dimensional steady-state basic profile, into a new theory which is concerned with small-amplitude perturbations superimposed upon a steady two-dimensional field. In so doing, the many and often questionable assumptions related with the so-called parallel-flow approximation are relaxed and the linear instability of nonparallel basic states may be analysed. The penalty to be paid in resolving two spatial dimensions is the need for numerical solution of a partial-derivative-based eigenvalue problem instead of the straightforward ordinary-differential-equation-based system of the Orr-Sommerfeld and Squire equations [6]. One of the early successes of the nonparallel two-dimensional linear instability analysis was the discovery of inviscid short-wave instability of two-dimensional eddies by Pierrehumbert [18] while the first viscous linear analysis in two non-periodic spatial dimensions known to us is the work of Lee *et al.* [16] on the instability of flow in a rectangular enclosure under the influence of gravity and temperature gradient. More recent viscous analyses, in step with

modern developments in algorithms and hardware, have been presented in [23] where we discuss the linear instability of two nonparallel flows, that in a rectangular duct and that in the infinite-swept attachment-line boundary layer. The nonparallel linear instability of laminar flows encompassing a recirculation bubble has been discussed by Barkley *et al.* [4] for flow behind a backward-facing step and by Theofilis *et al.* [29] for two separated boundary layer flows developing under the influence of adverse pressure gradients.

We re-interpret the transient solution $\mathbf{q}$ in three-dimensional physical space as one composed of small-amplitude three-dimensional perturbations $\tilde{\mathbf{q}} = (\tilde{u}, \tilde{v}, \tilde{w}, \tilde{p})^{\mathrm{T}}$ superimposed upon $\bar{\mathbf{q}} = (\bar{u}, \bar{v}, \bar{w}, \bar{p})^{\mathrm{T}}$, the latter again taken to be two-dimensional. Linearisation about $\bar{\mathbf{q}}$ is permissible on account of the smallness of perturbations compared with the steady-state $\bar{\mathbf{q}}$ and the resulting system for the determination of $\tilde{\mathbf{q}}$ is separable in both t and z on account of the steadiness and the two-dimensionality of the basic flow $\bar{\mathbf{q}}$. Eigenmodes are introduced in these directions such that

$$\tilde{\mathbf{q}}(x, y, z, t) = \hat{\mathbf{q}}(x, y)\, \mathrm{e}^{\mathrm{i}\,[\beta z - \omega t]} + c.c. \tag{5}$$

with $\hat{\mathbf{q}} = (\hat{u}, \hat{v}, \hat{w}, \hat{p})^{\mathrm{T}}$ and $\hat{w}$ being the disturbance velocity component in the z-direction. Complex conjugation is introduced in (5) since $\tilde{\mathbf{q}}$ is real while all three of $\hat{\mathbf{q}}, \beta$ and ω may be complex. In the framework of a temporal linear nonparallel instability analysis used presently we write the linearised system in the form of an eigenvalue problem for the complex quantity ω, while β is taken to be a real wavenumber parameter describing an eigenmode in the z-direction. The real part of ω is related with the frequency of the instability mode while its imaginary part is the growth/damping rate; a positive value of $\omega_{\mathrm{i}} \equiv \Im\{\omega\}$ indicates exponential growth of the instability mode $\tilde{\mathbf{q}}$ in time t while $\omega_{\mathrm{i}} < 0$ denotes decay of $\tilde{\mathbf{q}}$ in time. In the present framework the three-dimensional space comprises Ω extended periodically in z and characterised by a wavelength L_z in this direction which is associated with the wavenumber of each eigenmode, β, through $L_z = 2\pi/\beta$.

The system for the determination of ω and $\hat{\mathbf{q}}$ takes the form of a complex nonsymmetric generalised eigenvalue problem

$$[\mathcal{L} - (\mathcal{D}_x \bar{u})]\,\hat{u} - (\mathcal{D}_y \bar{u})\hat{v} - \mathcal{D}_x \hat{p} \;=\; -\mathrm{i}\,\omega\,\hat{u}, \tag{6a}$$

$$-(\mathcal{D}_x \bar{v})\hat{u} + [\mathcal{L} - (\mathcal{D}_y \bar{v})]\,\hat{v} - \mathcal{D}_y \hat{p} \;=\; -\mathrm{i}\,\omega\,\hat{v}, \tag{6b}$$

$$-(\mathcal{D}_x \bar{w})\hat{u} - (\mathcal{D}_y \bar{w})\hat{v} + \mathcal{L}\hat{w} - \mathrm{i}\,\beta\hat{p} \;=\; -\mathrm{i}\,\omega\,\hat{w}, \tag{6c}$$

$$\mathcal{D}_x \hat{u} + \mathcal{D}_y \hat{v} + \mathrm{i}\,\beta\hat{w} \;=\; 0, \tag{6d}$$

subject to appropriate boundary conditions on $\partial\Omega$. The linear operator $\mathcal{L} = (1/Re)$ $\left(\mathcal{D}_x^2 + \mathcal{D}_y^2 - \beta^2\right) - \bar{u}\mathcal{D}_x - \bar{v}\mathcal{D}_y - \mathrm{i}\,\beta\bar{w}$ with $\mathcal{D}_x = \partial/\partial x$, $\mathcal{D}_x^2 = \partial^2/\partial x^2$, $\mathcal{D}_y = \partial/\partial y$ and $\mathcal{D}_y^2 = \partial^2/\partial y^2$. Some details of an efficient numerical algorithm for the solution of the matrix eigenvalue problem resulting from numerical discretisation of the spatial directions x and y have been presented in [23].

Comparison of (1-2) and (5) reveals that the two formalisms are related in the limit $\beta \to 0$. However, $\hat{w}$ is not taken *a priori* to vanish within the framework of nonparallel linear instability; three-dimensionality of physical space is preserved and the existence of a two-dimensional steady-state solution $\bar{\mathbf{q}}$ is the result of $\tilde{\mathbf{q}} \to 0$ as $t \to \infty$. The comparison of (1-2) and (5) highlights two further key ideas of the present paper. On the one hand, the residuals discussed earlier acquire the physical interpretation of one of the linear eigenmodes which pertain to the steady-state $\bar{\mathbf{q}}$ and have $\beta = 0$; on the other hand, the rate of decay of the residuals σ is nothing but the damping rate ω_i of this linear perturbation, as delivered by numerical solution of the partial-derivative eigenvalue problem (6a-6d). Another question naturally arising concerns the physical behaviour of the system when the least stable member of the linear eigenspectrum which pertains to $\bar{\mathbf{q}}$ and has $\beta = 0$ becomes unstable. The answer is clearly that the existence of an unstable $(\beta = 0)$−eigenmode is

mutually exclusive with the ability to obtain a converged $\bar{\mathbf{q}}$. From the point of view of the global linear instability theory based on the partial derivative eigenvalue problem (6a-6d) the unsteady behaviour of two-dimensional flow may be related to $(\beta = 0)-$eigenmodes approaching conditions of neutral stability and interacting nonlinearly.

The answer to the second question posed in the Introduction may now also be obtained without reference to a specific flow example. The existence of a steady-state $\bar{\mathbf{q}}$ in a 2D numerical simulation is synonymous with the fact that all $(\beta = 0)-$eigenmodes of the flow have $\omega_i < 0$. Modes having $\beta \neq 0$, on the other hand, may be either growing or decaying linearly. In case $\omega_i < 0 \; \forall \; \beta$, a three-dimensional numerical simulation performed at some parameters in a three-dimensional domain defined by Ω and an *arbitrary* periodic extent L_z in the z-direction will deliver *identical* results for a converged $\bar{\mathbf{q}}$ compared with that of a two-dimensional simulation performed at the same parameters in the domain Ω. The situation changes in case a bracket of wavenumbers $\beta \in [\beta_1, \beta_2]$ exists which corresponds to unstable modes. The largest wavenumber β_2 defines a length $L_{z2} = 2\pi/\beta_2$; if the three-dimensional simulation is performed with $L_z < L_{z2}$ again no difference is to be expected between its result for $\bar{\mathbf{q}}$ and that of a two-dimensional simulation. Both will converge to the same steady-state solution $\bar{\mathbf{q}}$ since all wavenumbers of modes defined by an L_z constrained as above correspond to $\omega_i < 0$. However, if $L_z > L_{z2}$ at least one mode in the three-dimensional simulation will be unstable, which will result in the two- and three-dimensional simulations producing different solutions.

We return to the observation of oscillatory behaviour of the residuals near convergence and differentiate between exponentially decaying residuals of either sinusoidal or apparently nonlinear nature. A linear decay of $\ln[\mathbf{q}^t]$ is a consequence of $(\beta = 0)-$linear eigenmodes being stationary, i.e. having $\omega_r \equiv \Re\{\omega\} = 0$. However, other stable two-dimensional member of the eigenspectrum of $\bar{\mathbf{q}}$ need not correspond to stationary modes; damped

travelling modes having $\omega_r \neq 0$ will manifest themselves in the time-accurate simulation as residuals of sinusoidal character the magnitude of which decays exponentially. On the other hand, the unambiguously linear dependence of $\ln[\mathbf{q}^t]$ on t in the neighbourhood of $\bar{\mathbf{q}}$ is the consequence of the existence of a spectrum comprising modes which are clearly separated in parameter space from one another. The co-existence of several two-dimensional eigenmodes of approximately the same damping rate can lead to their nonlinear interaction and difficulty to observe a behaviour governed by nonparallel linear instability theory. Comparison of power spectral analysis of the time-dependent DNS signal and the results of the partial-derivative eigenvalue problem (6a-6d) may shed light upon the two-dimensional eigenmodes involved in such a nonlinear interaction.

2.4. On the time of integration until convergence

Straightforward rearrangement of (1-2) delivers an estimate of the time necessary (under linear conditions) for the least stable global mode present in the numerical solution to be reduced from an amplitude A_1 to A_2, which may be calculated from

$$T_{A_1/A_2} = \ln(A_1/A_0)/(-\omega_i), \tag{7}$$

where ω_i is the damping rate of the mode in question. The worst case scenario in a time-accurate integration is that the solution will be attracted by the least-stable global eigenmode developing upon $\bar{\mathbf{q}}$ and having $\beta = 0$ throughout the course of the simulation. An upper bound for the time necessary for the steady-state to be obtained may then be offered by (7) in which ω_i is the damping rate of this mode. Defining, for example, convergence as the reduction of an $O(1)$ residual by 10 orders of magnitude results in an integration time of $T_{10^{-10}} \approx 23/|\omega_i|$. This is a conservative estimate since it is occasionally observed that other stronger damped eigenmodes will come into play early in the simulation and the least-damped eigenmode will only determine the late stages of the convergence process.

An associated point concerns the misconception which often exists that initialising the numerical solution for $\bar{\mathbf{q}}$ at some Reynolds number from a state which is 'close' to the one desired, for instance using the converged solution at a somewhat different Reynolds number, may reduce the integration time. In the context of the present analysis this is shown to be a misplaced expectation. If there exists an $O(1)$ deviation between the target solution and its initial estimate, the deviation has to be reduced in magnitude during an integration of the equations of motion for the length of time determined by the least damped two-dimensional $(\beta = 0)$−eigenmode at the specific Reynolds number. It is this eigenmode of the flow and not the initial state which determines the length of the integration time for $\bar{\mathbf{q}}$. The ideas discussed in §2.3, on the other hand, lead to an algorithm application of which may save substantial amounts of the integration time necessary for reduction of residuals to machine-roundoff level.

2.5. Recovery of the converged solution $\bar{\mathbf{q}}$ from transient data

Having identified small-amplitude residuals in the calculation as the least damped global two-dimensional eigenmodes of the flow, it is now possible to utilise this information in order to recover the converged steady-state solution from transient data, without having to pursue the time integration of the equations of motion until convergence in time is obtained. Combining (1), (2) and (5) one obtains

$$\mathbf{q}(x, y, t) = \bar{\mathbf{q}}(x, y) + \varepsilon \left[\hat{\mathbf{q}}_r \cos \omega_r t - \hat{\mathbf{q}}_i \sin \omega_r t \right] e^{\sigma t}, \tag{8}$$

where $\hat{\mathbf{q}}_r \equiv \Re\{\hat{\mathbf{q}}\}, \hat{\mathbf{q}}_i \equiv \Im\{\hat{\mathbf{q}}\}$ and $\hat{\mathbf{q}}$ is one of the $(\beta = 0)$−linear eigenmodes in (5). It should be stressed here that the following discussion is applicable to transient data for which (8) holds, namely, solutions for which the entire time-dependence of the solution is exhibited in the residuals; in other words, the present analysis is based on the self-consistent premises that $\partial \bar{\mathbf{q}} / \partial t = 0$. Further, it is noted that $\hat{\mathbf{q}}$ may but need not be the

least-damped member of the eigenspectrum of $\bar{\mathbf{q}}$; the only prerequisite for the validity of the following discussion is that the transient solution has reached a regime of exponential decay of residuals. A final point is that the signal near convergence need not be composed of a single damped eigenmode as (8) implies. However, the elements of the theory for the recovery of $\bar{\mathbf{q}}$ from a signal being composed of several stationary ($\omega_r = 0$) and travelling ($\omega_r \neq 0$) linearly damped eigenmodes may be exposed by reference to (8) on which we focus our attention.

The calculation of $\bar{\mathbf{q}}$ from transient data for $\mathbf{q}$ follows in two stages. First, elementary signal analysis techniques deliver the results for ω_r and σ. Second, once ω_r and σ have converged in time (8) may be used to calculate $\bar{\mathbf{q}}$. The circular frequency ω_r is calculated from the the period of oscillations in the time-signal of $\mathbf{q}$ which, in turn, is identified by the maxima in the signal. Independently, in order to calculate σ we re-write (8) as

$$\frac{\partial^3 \mathbf{q}}{\partial t^3} + (\sigma^2 + \omega_r^2)\frac{\partial \mathbf{q}}{\partial t} - 2\sigma\frac{\partial^2 \mathbf{q}}{\partial t^2} = 0. \tag{9}$$

This expression may be evaluated at those times that $\partial \mathbf{q}/\partial t = 0$ in the course of the time-integration, i.e. at the same times that ω_r is calculated. At these times the magnitude of σ is given by

$$\sigma = \frac{1}{2}\frac{(\partial^3 \mathbf{q}/\partial t^3)}{(\partial^2 \mathbf{q}/\partial t^2)}\Big|_{(\partial q/\partial t)=0}. \tag{10}$$

In case $\omega_r = 0$, a monotonic dependence of $\partial \mathbf{q}/\partial t$ on t is usually observed from the beginning of the calculation until convergence, with $\partial \mathbf{q}/\partial t = 0$ only at convergence. In this case, the magnitude of σ may be calculated using

$$\sigma = \frac{(\partial^2 \mathbf{q}/\partial t^2)}{(\partial \mathbf{q}/\partial t)}. \tag{11}$$

With σ and ω_r converged in time (8) may be written as a linear system of three equations at three times $t_1 = t, t_2 = t + \Delta t$ and $t_3 = t + 2\Delta t$ for three unknowns, $\bar{\mathbf{q}}, \hat{\mathbf{q}}_r$ and $\hat{\mathbf{q}}_i$ with

the transient solution $\mathbf{q}_n \equiv \mathbf{q}(x, y, t_n)$ known at these times. Simple algebra delivers the desired converged steady-state solution $\bar{\mathbf{q}}$ as

$$\bar{\mathbf{q}} = \frac{\mathbf{q}_1\, e^{2\sigma\Delta t} - 2\, \mathbf{q}_2\, e^{\sigma\Delta t} \cos\omega_r\Delta t + \mathbf{q}_3}{e^{2\sigma\Delta t} - 2\, e^{\sigma\Delta t} \cos\omega_r\Delta t + 1}. \tag{12}$$

As an aside, the spatial structure $(\hat{\mathbf{q}}_r, \hat{\mathbf{q}}_i)$ of the linear eigenmode $\hat{\mathbf{q}}$ may also be recovered to within an arbitrary constant from the same linear system. Equivalently, if only the converged steady-state solution is of interest, the expression

$$\bar{\mathbf{q}} = \frac{1}{\omega_r^2 + \sigma^2} \left\{ (\omega_r^2 + \sigma^2)\mathbf{q} - 2\sigma\frac{\partial \mathbf{q}}{\partial t} + \frac{\partial^2 \mathbf{q}}{\partial t^2} \right\} \tag{13}$$

may be used for the recovery of $\bar{\mathbf{q}}$ from transient data for $\mathbf{q}$ and its first two time-derivatives. Either of (12) or (13) may be used for the cases of residuals corresponding to stationary ($\omega_r = 0$) or travelling ($\omega_r \neq 0$) single linear eigenmodes.

This idea may be extended to extract $\bar{\mathbf{q}}$ from a DNS signal comprising several linearly decaying eigenmodes superimposed upon the steady-state solution,

$$\mathbf{q} = \bar{\mathbf{q}} + \sum_n \varepsilon_n(q_{n,r} \cos\omega_{n,r}t - q_{n,i} \sin\omega_{n,r}t)e^{\sigma_n t}. \tag{14}$$

As an example, in the case of one stationary

$$\varepsilon_1 \mathbf{q}_{1,r} e^{\sigma_1 t} \tag{15}$$

and one travelling

$$\varepsilon_2(\mathbf{q}_{2,r} \cos\omega_r t - \mathbf{q}_{2,i} \sin\omega_r t)e^{\sigma_2 t} \tag{16}$$

linear disturbances being present in the signal, one may first extract information for the damping rate of the stationary mode from the signal itself and for the damping rate and frequency of the travelling disturbance from the first time-derivative of the DNS signal for $\mathbf{q}$. Subsequently, one may solve the $(2NxNy) \times (2NxNy)$ system defined by writing

$$(\sigma_2^2 + \omega_r^2)\bar{\mathbf{q}} + (\sigma_1^2 + \sigma_2^2 + \omega_r^2 - 2\sigma_1\sigma_2)\varepsilon_1\mathbf{q}_{1,r}e^{\sigma_1 t} =$$

$$\frac{\partial^2\mathbf{q}}{\partial t^2} - 2\sigma_2\frac{\partial\mathbf{q}}{\partial t} + (\sigma_2^2 + \omega_r^2)\mathbf{q} \qquad (17)$$

at two consecutive times t_1 and t_2 for $\bar{\mathbf{q}}$ and $\varepsilon_1\mathbf{q}_{1,r}$, where Nx and Ny are the number of points discretising the $x-$ and $y-$spatial directions, respectively.

The accuracy by which ω_r and σ are determined depends on that by which the first three time-derivatives of $\mathbf{q}$ are calculated; this, in turn, depends on the time-step in the calculation and the number of fields stored in order for backward differentiation formulae to be applied. Since the time-step is controlled by CFL considerations, it is advisable to store a reasonably high number of fields in order for high accuracy of ω_r and σ and, in turn, of $\bar{\mathbf{q}}$ to be obtained. The calculations to be presented in what follows have been performed using five-point backward differencing formulae on an equidistant grid [14].

At conditions at which a steady-state solution exists most two-dimensional global eigenmodes of the converged steady-state are heavily damped ($\sigma_n = O(1)$ in equation (14)). Consequently, if the time-integration of the equations of motion is pursued long enough, only a handful of $(\beta = 0)-$global eigenmodes will survive and persist in the DNS signal. Clearly, it is the least damped of the global instabilities that will determine the ultimate behaviour of the solution. In determining whether one integrates the equations of motion until all but the least-damped of the eigenmodes have subsided in order to apply (12) or (13) or one recovers $\bar{\mathbf{q}}$ at an earlier time from a signal in which a number of damped eigenmodes still persist one should take into account the following factors.

First, the efficiency of the specific DNS algorithm determines whether the cost of integrating the equations of motion until convergence is acceptable at given flow parameters. The cost of computing ω_r, σ, intermediate values of $\bar{\mathbf{q}}$ and monitoring convergence of

all these quantities, possibly for several eigenmodes, must also be weighed against the straightforward approach of pursuing the time-integration in the DNS until convergence. However, at all Reynolds numbers studied in the prototype flow monitored both σ and ω_r of individual modes have converged within the first quarter to half of the total integration time, making further time-integration superfluous. While the integration time until convergence is short at low Reynolds numbers, on account of large damping rates of the least-damped linear eigenmodes, at increasingly large Reynolds numbers the magnitude of the damping rates becomes increasingly smaller and application of the ideas exposed in this section becomes increasingly attractive in order for substantial savings in computing effort to be materialised.

3. RESULTS FOR THE SQUARE LID-DRIVEN CAVITY

An example flow in which these ideas may be illustrated is the classic lid-driven cavity [2]. In its function as a testbed for numerous algorithms this flow has generated a substantial amount of information which is relevant to the preceding discussion. Calculations for $\bar{q}$ were performed using a two-dimensional spectrally-accurate algorithm for direct numerical simulation of flow in nonperiodic geometries. The code is based on a real-space eigenvalue-decomposition of the spectral collocation differentiation matrices extending ideas discussed by Ku *et al.* [8] and uses one member of the low-storage second-order accurate time-integration schemes put forward by Spalart *et al.* [17]. A spectral algorithm was chosen in order for optimal accuracy to be obtained on a low number of collocation points, the latter being dictated by the maximum number of points on which numerical solution of the partial-derivative eigenvalue problem is feasible using current computer technology. Solutions were obtained using Jacobi polynomials for the spatial discretisation at resolutions depending on the Reynolds number and ranging from 32^2 to 128^2 spectral collocation points. The time-steps at the different Reynolds numbers were kept well below those

dictated by the CFL condition in order for reasonable accuracy of the results of σ to be ensured. In view of our arguments being based on nonparallel linear instability analysis and the well-known sensitivity of linear instability analysis results on the accuracy of the basic flow, we first present a validation of both the basic flow and the partial derivative eigenvalue problem.

3.1. Validation studies

The accuracy of the converged steady-state solutions is first assessed by comparison with the established works of Ghia *et al.* [27] and Schreiber and Keller [19]. Converged basic states have been calculated at several Reynolds numbers of which we present calculations at $Re = 400, 1000, 3200$ and 4000, the first three obtained on 32^2 and the last on 48^2 Legendre collocation points. At $Re = 400$ and 1000 both aforementioned works present results while at the higher Reynolds numbers we compare our calculations individually with either work. Interestingly, aside from the locations and maximum values of streamfunction and vorticity in the primary vortex core, Schreiber and Keller [19] analysed and presented their results in the form of a converging series calculated by Richardson extrapolation. Comparisons are presented in a twofold manner. The comparison of our calculations for the location and maxima in the stream-function $\bar{\psi}$ and the vorticity $\bar{\zeta}$ with those of the reference works is shown in Table 1a; note that [19] define ζ to have an opposite sign to that of [27] and the present work. Although the overall agreement of all results is quite reasonable marginal differences exist. These may be attributed to the different grids used in all three works, making an interpolation procedure necessary for detailed comparisons. To this end, we employed a piecewise cubic procedure to transfer our results onto the (different) maxima of the benchmark calculations. Our interpolated values as well as the results of [27] and [19] are presented in Table 1b, where the individual comparisons demonstrate a substantially more satisfactory agreement of our calculations with both benchmark works

at low Re−values and especially with the Richardson extrapolated results of [19] at the highest Reynolds number monitored.

It is well-known from comparisons of three-dimensional DNS results and one-dimensional Orr-Sommerfeld-based linear instability analysis that details of the steady basic state strongly influence the accuracy of the growth/damping rates of linear eigenmodes [12]. The remaining differences between our results for the two-dimensional steady-states in the lid-driven cavity and those of the benchmark works are next assessed in this light, from the point of view of their influence on the global linear instability analysis results. Two solutions of the partial derivative eigenvalue problem (6a-6d) for the lid-driven cavity exist, those of Ramanan and Homsy [21] (RH) and Ding and Kawahara [5] (DK). These authors have presented linear instability analyses of the square lid-driven cavity flow which deliver consistent results at low Re but predict different critical Reynolds number values for linear amplification of three-dimensional perturbations. While individual comparisons are certainly possible, at high Reynolds numbers neither work presents results for the two-dimensional global linear instabilities which are central to the theme of the present paper. We therefore refrain here from discussion of three-dimensional linear instability and the issue of a linear critical Reynolds number and monitor a low value of the Reynolds number, $Re = 200$, at which both RH and DK present results at $\beta = 0$.

Table 2 shows the tabulated values of RH, the graphically reproduced results of DK and our solutions of the partial-derivative eigenvalue problem (6a-6d). The overall agreement of the previous and the present instability analyses is quite good and all results indicate the experimentally established fact of stability of the two-dimensional flow in the lid-driven cavity at this Reynolds number [2]. Regarding the quality of the basic flow, it may be inferred from the results of Table 2 that the basic states of both RH and DK and the present

work are practically identical for the purposes of the linear instability analysis that follows, at least at the Reynolds numbers discussed.

3.2. Numerical residuals and ($\beta = 0$) linear eigenmodes in the square lid-driven cavity

Figs. 1-4c show the convergence histories of the two-dimensional DNS at several Reynolds numbers, with the qualitative behaviour of residuals discussed earlier observed. The convergence of the rate of decay of residuals σ, calculated using (3-4), is shown in Table 3 at $Re = 100, 200$ and 300. Also shown is the damping rate ω_i of the least-damped eigenmode having $\beta = 0$ as obtained by linear analysis, based on the partial-derivative eigenvalue problem (6a-6d), of the converged steady-state $\bar{q}$ corresponding to each Reynolds number. The excellent agreement between the two quantities leaves lit-tle room for doubt that numerical residuals may be identified as being the least-damped $(\beta = 0)$–eigenmode of the corresponding converged steady-state. It is interesting to note here that such an agreement could *not* be obtained when we followed the commonly-used procedure to terminate the steady-state calculation after a decay of residuals by an arbitrar-ily defined seemingly adequate small number of orders of magnitude, say 5-6. Such poorly converged in time basic states may be viewed as comprising a small unsteady component the linear instability analysis of which is bound to deliver erroneous results. Further, it is worth mentioning that the prediction (7) of the time necessary to integrate the equations of motion until convergence in time is in line with the results of Table 3 and Fig. 1.

A clearly defined single value of σ which determines the behaviour of residuals in the entire course of the time-integration is a result of a two-dimensional eigenspectrum of $\bar{q}$ in which the least damped two-dimensional $(\beta = 0)$–eigenmodes are stationary and well separated in parameter space from their more stable counterparts. The situation becomes more intricate, but still amenable to analysis, as the Reynolds number increases. Qualitative differences may be found between the results of Figs. 1, 2 and 3, although all simulations

were started from the same initial condition $\psi = \zeta = 0$; we discuss the differences between the results of Figs. 1 and 3 first. While in both sets of results a short initial transient is followed by exponential decay of residuals, in the first set this decay pursues at the same rate for almost two decades while in the second two different rates of exponential decay of residuals are demonstrated. Inspection of the full spectra delivered by numerical solution of (6a-6d) at each Reynolds number reveals that as the Reynolds number increases an increasingly larger number of eigenmodes, both stationary and travelling appear in the eigenspectrum of $\bar{q}$, having damping rates approximately equal with that of the least damped eigenmode. As a consequence, the numerical solution may initially be attracted to a different than the least damped $(\beta = 0)$−eigenmode but its long-time behaviour will be determined by the latter disturbance. In both the $Re = 500$ and the $Re = 1000$ results of Fig. 3 the damping rates ω_i of the least and the next more stable mode are presented as symbols superimposed upon the curves used to determine σ. The results at $Re = 400$, on the other hand, are a qualitatively different manifestation of the same phenomenon of a dense eigenvalue spectrum in the neighbourhood of the least stable $(\beta = 0)$−eigenmode of $\bar{q}$. Instead of the solution being attracted by two distinct linear eigenmodes for long integration times, here the progression between a q initially attracted by the third least stable member of the eigenspectrum of $\bar{q}$ to the final state (which is again determined by the least stable eigenmode) is gradual, taking place throughout the entire convergence history. The result is the barely perceptible deviation from an exponential decay of residuals which may be seen in the result for the time dependence of $\log\{\psi^t\}$ at this Reynolds number, presented in Fig. 2.

Yet another qualitatively different behaviour is observed in the time-signal of q as a consequence of a further increase of the Reynolds number. Alongside the least damped stationary mode travelling disturbances appear, as seen in the results of Figs. 4a-4c. In all

three figures $\sigma(t)$ assumes the form of exponentially decaying disturbances. However, while at the lowest Reynolds number a clearly identifiable sinusoidal perturbation may be seen, having $\omega_r \approx 0.97 \pm 0.01$, a barely perceptible deviation from a single oscillatory disturbance ($\omega_r \approx 0.954 \pm 0.012$) may be seen at $Re = 5000$; at $Re = 7500$ the solution demonstrates a behaviour which might be interpreted either as nonlinearity or as superposition of two exponentially decaying linear sinusoidal disturbances having frequencies of $\omega_r = 0.933$ and 0.945. In order to analyse these observations we pursue two independent paths. First, we perform a nonparallel linear instability analysis of the converged steady state at each Reynolds number and monitor the least-stable member of the eigenspectrum, which turns out to be a stationary linear eigenmode. Second, we perform a discrete Fourier transform (DFT) of the DNS signal for q at $Re = 2500, 5000$ and 7500 and compare the results with the eigenvalues of the travelling disturbances delivered by the linear instability analysis.

Table 4 shows that a progressive deviation of the rate of decay of the residuals from the damping rate of the least-damped eigenmode occurs as Re increases. This result suggests that as the Reynolds number increases nonlinear interaction of the least stable eigenmodes may cause a departure of the numerical solution from a behaviour predicted by nonparallel linear theory. The role that the least stable members of the full eigenvalue spectrum play in the dynamics of the flow may be inferred from the results of Figs. 5a- 5c. In Fig. 5a we present the DFT of the DNS signal for $\psi(0.5, 0.5)$ scaled by the maximum value of the spectral density. A single peak at $2\pi f \approx 1$, albeit of somewhat wide support, dominates over two much smaller peaks at $2\pi f = 0$ and $2\pi f \approx 2$. Shown are also the results of (6a-6d) for ω_r, arbitrarily placed on the vertical axis for readability. An one-to-one correspondence between the peaks in the spectrum and the values of ω_r for stationary and travelling linear eigenmodes is clearly identifiable. Interestingly, the width of the support of the peaks is found to be associated with the existence of more than one eigenvalues in

the partial-derivative eigenvalue problem spectrum, at both $\omega_r \approx 1$ and $\omega_r \approx 2$. The origin of the existence of only harmonics of the first travelling eigenmode in the full eigenvalue spectrum deserves further investigation. It should be noted here that a Krylov subspace iteration method has been used for the solution of the partial-derivative eigenvalue problem, which results in only a window of the eigenvalue spectrum being captured at any single calculation. The number of converged eigenvalues recovered increases as the subspace dimension increases. However, the neighbourhood of $(\omega_r, \omega_i) = 0$ has been well resolved in all results presented here. A higher Krylov subspace dimension has been found to deliver additional eigenvalues at higher frequencies.

While the agreement between the frequencies in the DNS signal and those of the non-parallel linear analysis of the converged steady state is evident, the results of Fig. 5a do not provide any information on the damping rates ω_i of the disturbances whose frequency lies at $\omega_r \approx 1$ in relation to those at different frequencies. For our argument that the residuals in the calculation may be identified as the least stable of the two-dimensional $(\beta = 0)$–eigenmodes to be valid, the damping rate of the linear disturbances at $\omega_r \approx 1$ must be lower than that of modes with higher frequencies; this is a point to which we will return shortly. Qualitatively analogous results are obtained at $Re = 5000$, seen in Fig. 5b. Besides the slight shift towards lower frequencies, the quantitative difference with the results at $Re = 2500$ is that the strength of the eigenmodes at $\omega_r \approx 2$ is substantially larger than that of their counterparts at $Re = 2500$ in relation to the strength of the respective modes at $\omega_r \approx 1$; this is the origin of the slight deviation from a purely sinusoidal behaviour of the signal at this Reynolds number, seen in Fig. 4b. Further, additional eigenmodes appear alongside the counterparts of those seen at $Re = 2500$ at $\omega_r = 0$ and $\omega_r \approx 1$ and new modes appear at $\omega_r \approx 3$ and $\omega_r \approx 4$. Finally, at $Re = 7500$, the pattern discovered at the lower Reynolds number values qualitatively repeats itself, with the appearance of

additional modes at the same and new at high-frequencies; furthermore a new mode which does not fit in the period-doubling scenario discussed also is present in the linear instability analysis results, which the DFT reveals to be too weak to play an important role in the dynamics of the flow at this Reynolds number value.

We return to the question of damping rates of the linear instability modes and present in Fig. 6 the full spectrum of eigenvalues in the neighbourhood of $\omega = 0$ at $Re = 2500, 5000,$ and 7500. Results of significance in this figure are the following. First, as the Reynolds number increases the flow becomes less stable to two-dimensional linear $(\beta = 0)$—eigenmodes. Second, in all three Reynolds numbers the least stable modes are stationary disturbances. Third, perfect symmetry about $\omega_r = 0$ may be observed in the results, as should be expected from the ability to reformulate (6a-6d) as a real eigenvalue problem. Consistent with the DFT results of the signal discussed earlier, the eigenmodes at $\omega_r \approx 1$ are less stable than their counterparts at higher frequencies. Comparing, for example, the $Re = 5000$ eigenmodes $(\omega_r, \omega_i) = (0.967, -0.0158)$ and $(\omega_r, \omega_i) = (1.921, -0.0319)$ one finds that, if introduced at the same initial amplitude in the flow, the second mode would be reduced by a given number of orders of magnitude in amplitude in approximately half as long an integration time as that required for the first mode to experience the same reduction of amplitude.

3.3.   The critical Reynolds number of $(\beta = 0)$—linear disturbances

The preceding discussion leads to re-examination of the question of a critical Reynolds number for linear growth of two-dimensional global instabilities in the square lid-driven cavity. Consistent with well-established numerical solutions for the steady-state in this flow the nonparallel linear instability analysis results of § 3.2 deliver a least damped stationary $(\beta = 0)$—eigenmode which has a damping rate whose magnitude decreases with increasing Reynolds number. The dependence of ω_i on Re for this mode has been obtained at several

Reynolds numbers and is presented by symbols in Fig. 7. Analysis of the results for the damping rate of the least-damped eigenmode as function of the Reynolds number delivers a curve-fit of the data by using

$$\omega_i = -109.071 \, Re^{-1.068}. \tag{18}$$

The curve defined by (18) is also shown in Fig. 7 by a solid line and has been found to deliver reasonably accurate predictions of ω_i at $Re > 1000$, where the calculated data may be collapsed onto a single curve. The upper bound of the Reynolds-number range in which (18) may be used with confidence to predict the rate of decay of residuals and the associated time of integration of the equations of motion until a steady-state solution is reached must be $Re \approx 10^4$, a value below which a multitude of two-dimensional numerical solutions have demonstrated the existence of converged two-dimensional states. In the framework of the current nonparallel linear instability analysis this should manifest itself by $\bar{q}$ losing its stability in a linear framework to amplified two-dimensional perturbations having $\beta = 0$. However, as has been mentioned, the existence of a converged steady-state solution is synonymous with all global eigenmodes of the flow being stable. Another possibility is that the nonlinear interaction of two-dimensional global neutrally-stable disturbances as the Reynolds number increases may be held responsible for the observed inability to obtain a converged steady state solution. However, from (18) it follows that $\omega_i < 0$, $\forall Re$ and the flow remains stable to all two-dimensional $(\beta = 0)$–eigenmodes. Two aspects of this prediction should be stressed here. First, (18) is a curve-fit, at best valid up to the highest Reynolds number used to produce it, $Re = 7500$. Second, the filling-up of the eigenspectrum and the associated nonlinear interaction of some of the least stable eigenmodes as the Reynolds number increases, causes a systematic departure of the numerical solution for $\mathbf{q}$ from one determined by a single eigenmode of the nonparallel linear instability theory, as already shown in the results of Table 4. On the other hand, the trend predicted by (18) is

correct, namely that the damping rates of two-dimensional global linear instabilities as Re increases are exponentially small in magnitude. As such, an increasingly large number of global modes may be considered neutrally stable at large Reynolds numbers; it is therefore likely that the second scenario, namely nonlinear interaction of near neutrally stable two-dimensional global flow eigenmodes is responsible for the observed loss of ability to obtain a steady-state solution of the equations of motion at $Re > 10^4$ (f.e. [31]).

3.4. The spatial distribution of the least-damped global eigenmode

A closer look at the spatial distribution of the least-damped of the global linear eigenmodes, which we have identified as the residual of the DNS calculation at low and moderate Reynolds numbers, is now in order. Before presenting results of the eigenvalue problem at a single Reynolds number value, $Re = 1000$, we remark that the converged two-dimensional flow $\bar{\mathbf{q}}$ in the lid-driven cavity has two velocity components $\bar{u}$ and $\bar{v}$ both of which lie on the plane Ω. Consequently, there is no preferential direction along the z-spatial coordinate. Mathematically, this physical fact is expressed by the ability to write (6a-6d) as an eigenvalue problem with real coefficients which admits either real or complex-conjugate pairs of solutions. The former are identified as the stationary and the latter as the travelling modes. In the case of flow at $Re = 1000$ the least damped eigenmode is a stationary disturbance whose eigenvalue is $\omega = (0.0, -0.068)$. Fig. 8 shows the scaled disturbance eigenvector as contour-lines, the labelling of which is to be found in Table 5.

The most striking feature of the results for $\hat{u}$ and $\hat{v}$ is that these disturbance velocity components qualitatively correspond to small-perturbations of their basic flow counterparts $\bar{u}$ and $\bar{v}$, respectively. The predominant motion set up by the disturbance flowfield follows that of the basic flow with flow being driven along the positive $x-$axis by $\hat{u}$ in the top half of the cavity and along the opposite direction in the lower half. Analogously, $\hat{v}$ divides the cavity in two parts; one in which flow is along the positive and one along the

negative $y-$direction; this result may be visualised in Fig. 8. Another interesting result clearly visible in both the $\hat{u}$ and the $\hat{v}$ velocity components is the existence of local vortical motion in the neighbourhood of all four corners of the cavity. As has been mentioned, the three-dimensionality of physical space is respected in the framework of the nonparallel linear instability analysis, with the existence of a steady-state solution $\bar{q}$ being associated with a damped eigenmode which may possess a nonzero spanwise disturbance velocity component $\hat{w}$; that of flow at $Re = 1000$ is shown in Fig. 8. It should be mentioned here that the spatial structure of $\hat{w}$ of the present two-dimensional $(\beta = 0)-$eigenmode is qualitatively reminiscent of that of its three-dimensional $(\beta \neq 0)-$counterparts discussed by Ding & Kawahara [5] at approximately the same Reynolds number value. Finally, the disturbance pressure $\hat{p}$ also inherits the qualitative characteristics of the basic flow, with remarkable analogies existing between the basic flow pressure [2] and the present linear instability analysis result. The flowfield pattern set up by combination of the $\hat{u}$ and $\hat{v}$ disturbance velocity components is visualised in Fig. 9.

Of the multitude of results on spurious and transient solutions of the two-dimensional incompressible continuity and Navier-Stokes equations, we recall here those of Schreiber and Keller [20] and E and Liu [30], respectively. The former investigators demonstrated that a steady-state formulation of the governing equations may, on occasion, deliver unphysical results which persist when using different spatial discretisation schemes but not at different resolutions. While speculative, on account of the impossibility of direct comparisons of results of steady and unsteady calculations, a plausible argument may be put forward here that the combination of the particular initial conditions and resolution used in the steady calculations result in the gross features of one or more of the global linear eigenmodes being well resolved at that resolution. Since the time-dependence which would ensure the exponential decay of the eigenmode at the Reynolds number values studied in [20] is

absent from the scheme integrating the steady equations of motion, the iteration merely serves to converge to a solution which is close to the initial attractor. A higher resolution is no guarantee of preservation of the same initial condition, resulting in the irreproducibility of the behaviour at the lower resolution and the characterisation of the latter as spurious. E and Liu [30], on the other hand, compare different schemes for the spatial discretisation used within time-accurate solutions and present results at given times. Some of the results which these researchers present at $Re = 10^4$ are at a rather early time in terms of that necessary for convergence at this Reynolds number value (Fig.4, p.129, streamlines at $t = 2$). In these results one may interpret the states presented as superposition of several global eigenmodes which can be present at an $O(1)$ amplitude in the solution at this early time, upon the well-known steady-flow streamline pattern.

3.5. Obtaining the converged steady-state solution from non-converged transient data

The preceding discussion has demonstrated the association of residuals in two-dimensional incompressible DNS calculations with the two-dimensional global linear instability modes of the converged steady state. In this section we present examples of recovery of steady-state solutions from transient DNS data using this information and the algorithm of § 2.5. We stress that the applicability of the algorithm is intimately linked with the quality of the DNS and the initial conditions used for the simulation, since both determine when, for what length of time and to which linear eigenmode the time-accurate solution will be attracted in the course of the time-integration. Here we present a discussion of some parameters which affect the results returned by the algorithm in a few Reynolds number cases of those on which the algorithm was validated.

Results at $Re = 100, 400$ and 1000 are shown in Table 6; at each Reynolds number we have performed three sets of calculations, two direct numerical simulations and one solution of the partial-derivative eigenvalue problem. Both DNS start from the initial

condition $\psi = \zeta = 0$ for the flow streamfunction and vorticity, respectively. On the one hand, the converged 'exact' steady state $\bar{\mathbf{q}}$ has been calculated by marching the equations of motion until such a time $\bar{t}$ that the residuals were reduced to machine-roundoff level, using 64-bit arithmetic and monitoring convergence along the lines discussed in §3.1. On the other hand, we have run another DNS but marched the equations of motion until such a time $\tilde{t}$ was reached at which a linear regime was identified by the convergence in time of ω_r (when applicable) and σ. The time-marching was then interrupted and either (12) or (13) was solved for the respective 'estimated' steady-state solution $\tilde{\mathbf{q}}$. Finally, the partial-derivative eigenvalue problem (6a-6d) was solved for two-dimensional disturbances ($\beta = 0$) developing upon $\bar{\mathbf{q}}$ and the eigenvalue spectrum pertaining to the flow at each Reynolds number was recovered. The results were compared both in terms of the magnitude of the relative discrepancy of the two DNS-obtained solutions $\Delta \mathbf{q} \equiv |(\tilde{\mathbf{q}} - \bar{\mathbf{q}})/\bar{\mathbf{q}}|$ and by monitoring the difference between σ in the second set of DNS and ω_i. Table 6 shows the resolutions and time-steps used in several simulations, the time $\bar{t}$ at which a converged steady-state solution $(\bar{\psi}, \bar{\zeta})$ was obtained by DNS and the time $\tilde{t}$ at which the damping rate of residuals converged to within a predefined tolerance of relative discrepancy 10^{-6} between successive values of σ and the results for $\tilde{\psi}$ were calculated. The value of σ as well as the relative discrepancy $\Delta \tilde{\psi} \equiv |(\tilde{\psi}(\tilde{t}) - \bar{\psi})/\bar{\psi}|$ between the estimated and the exact steady-states is also shown; the level at which the eigenmode being damped is present in the transient solution at time $\tilde{t}$ may be inferred from $\Delta \psi$.

The most significant result of this table is the ratio $\tilde{t}/\bar{t}$. The case $Re = 100$ is typical of one in which the least-stable eigenmode determines the transient behaviour of the DNS throughout most of the time-integration process. With the results for σ converging quite quickly, the desired converged steady-state may be obtained at a time between a quarter at the coarsest and a fifth at the finest resolution of the time required by the time-marching

algorithm for the residuals to be eliminated. The result for σ is only marginally affected by resolution and time-step; the precise times at which σ converges are affected by a small amount when refining the grid, with the finest resolution results converging earlier. In all cases use of the algorithm of § 2.5 results in substantial savings compared with the otherwise necessary computing effort. The spatial distribution of the difference $\Delta\tilde{\psi}$, obtained using 48 collocation points to discretise each spatial direction, is shown in Fig. 10; aside from the level of $\Delta\tilde{\psi}$ it is interesting to notice that the discrepancy between the two solutions attains its maximum values in the centre of the cavity and neither the singularity of the boundary conditions nor the corner vortices are manifested in this quantity. The same qualitative behaviour was shown by all distributions of $\Delta\tilde{\psi}$ at lower resolutions. An estimate of the converged solution $\tilde{\psi}$ obtained by application of (12) at $\bar{t} = 15$ may be found in Fig. 11, drawn as contours at the levels presented by [27]. No cosmetic post-processing of the results has been applied, with values presented at the collocation points used. As it is to be expected by the results of Table 6 the agreement between $\tilde{\psi}$ and the result of [27] is remarkable.

The case of $Re = 400$ will be discussed shortly. At $Re = 1000$, σ converges at approximately the same fraction of total integration time as in the $Re = 100$ results. However, compared with the $Re = 100$ case where the discrepancy between estimated and converged steady-states is three to four orders of magnitude smaller compared with that shown by $\Delta\psi$, here only one order of magnitude difference between the maxima of $\Delta\tilde{\psi}$ and $\Delta\psi$ is shown. Though small, the discrepancy between $\tilde{\psi}$ and $\bar{\psi}$ is much larger than roundoff level, implying that elimination of the least stable eigenmode from the time-dependent signal for ψ at $Re = 1000$ does not suffice to deliver the desired $\bar{\psi}$. Another observation that may be made by comparing the results of the $Re = 100$ and $Re = 1000$ cases is that at approximately the same value of $\tilde{t}/\bar{t} \approx 0.23$, $\Delta\tilde{\psi}$ is higher by about an

order of magnitude at $Re = 1000$ compared with that at $Re = 100$. In searching for an explanation of this behaviour, three factors may be recalled. First, convergence of σ between successive values is a necessary but not sufficient condition for the algorithm of § 2.5 to deliver accurate results; the converged σ should be compared with the corresponding damping rates ω_i in the least-stable part of the eigenspectrum of the converged steady-state $\bar{q}$. Second, as the Reynolds number increases the damping rates of all global eigenmodes decrease, suggesting that increasingly longer integration times are necessary in the case of a higher Reynolds number in order for the residuals to subside to the same level as in a lower Reynolds number case. Third, the separation of the eigenvalues in the global spectrum plays a significant role in attracting the transient solution, as will be discussed with reference to the $Re = 400$ results. A distinction must be made between the early and the late stages of the transient behaviour of the DNS solution. In the latter it is the least-damped eigenmode which must eventually be damped in order for a steady-state to be obtained. During the early stages of the simulation, on the other hand, an arbitrary initial condition may need a large number of damped global eigenmodes in order to be reconstructed. It is, therefore, conceivable that at the early stages of the simulation a number of eigenmodes other than the least-damped one are present in the transient solution. However, as time progresses, increasingly more of these additional eigenmodes subside on account of their large damping rates, to the effect that only the least-damped mode remains to determine the behaviour of the residual. In other words, as time progresses, equation (14) reduces to (8) and the theory of § 2.5 focussing on a single damped eigenmode is applicable.

This conjecture may easily be put to test by simply permitting the time integration in the second DNS to proceed beyond $\tilde{t}$ while monitoring on the one hand σ against ω_i and on the other hand $\Delta\tilde{\psi}$ in the process; the results may be found in Table 7. Again we discuss the results at $Re = 100$ and 1000 first. At both the lower and the higher

Reynolds number further integration of the equations of motion in time results in all but the least-stable eigenmode being eliminated from the signal, as clearly demonstrated by the progressive agreement between the damping rate of residuals σ and the damping rate ω_i of the least stable $(\beta = 0)$−global flow eigenmode. Consistent with this result is the increasingly improved accuracy by which the algorithm of § 2.5 returns the estimate of the converged steady state, as shown by the minimum and maximum values of $\Delta\psi$ also cited. Interestingly, $\bar{\psi}$ may be recovered at the same low level of discrepancy in the two Reynolds number cases, f.e. $O(10^{-8})$ at $Re = 100, \tilde{t}/\bar{t} = .25$ and $Re = 1000, \tilde{t}/\bar{t} = .35$, although the agreement of σ with ω_i in the $Re = 100$ is about an order of magnitude better than that in the $Re = 1000$ case.

At $Re = 400$, as has already been shown in the results of Fig. 2, during the entire course of the time integration, the DNS does not lock on any of the eigenmodes of the flow. On account of the dense eigenspectrum in the neighbourhood of the least stable eigenmode, the integration is first attracted by the third least stable eigenmode from which it gradually departs as time progresses, approaching both the first and the second least stable eigenmodes. In the meantime continuation of the time-integration results in the converged steady state being reached before the linear eigenmodes come into play in a manner analogous to that observed at $Re = 100$ and 1000. While the results at $Re = 100$ and 1000 suggest that permitting the time-integration to proceed beyond the highest value of $\tilde{t}/\bar{t} = .35$ would yield even better agreement between the results for the estimated and the true steady-state solution, the analogous discrepancy at $Re = 400$ decays much slower. Rather than weakening the findings at the other two representative Reynolds numbers, the $Re = 400$ result is a strong demonstration that it is the precise details of the least stable part of the flow global eigenspectrum which govern the behaviour of the DNS; if the least-stable eigenmodes are clearly separated in the spectrum, as the case is at $Re = 100$

and $Re = 1000$, it is likely that a single eigenmode will attract the numerical solution in the course of the time integration, otherwise a dynamic behaviour of the DNS which is governed at least for part of the integration time by nonparallel linear instability theory may not be realised. In other words it is not largeness of Re but the details of the global eigenspectrum which determine whether nonparallel linear theory has a role to play in the dynamic behaviour demonstrated in the DNS.

3.6. Three-dimensionality as a consequence of amplified ($\beta \neq 0$) two-dimensional linear eigenmodes

Finally, we turn our attention to the differences between two- and three-dimensional simulations on account of growing global linear instability modes. While the physics behind the instability mechanisms is universal, the lid-driven cavity flow example serves again as a demonstrator, with the differences between two- and three-dimensional numerical simulation results in this flow being well established [8]. Here we call upon the global linear instability theory to discuss their straightforward explanation.

It is possible that while the ($\beta = 0$)−eigenmodes at a certain Reynolds number are damped there exist unstable $\beta \neq 0$ global flow eigenmodes. Indeed, Ding and Kawahara [5] have shown that at $Re = 950$ the flow is unstable to modes having $\beta \in [\beta_l, \beta_h]$ with $\beta_l = 2\pi/L_h \approx 6.6$ and $\beta_h = 2\pi/L_l \approx 8.3$, while the domain of unstable wavenumbers systematically broadens in both directions on the β−axis as the Reynolds number increases. There exist two possibilities of introduction of three-dimensionality by means of DNS, either by considering spanwise periodicity (pDNS) or by taking an aperiodic spanwise domain bounded by solid walls (aDNS). In the case of pDNS the integration domain in the spanwise direction is defined through discrete integer multiples of a fundamental wavenumber β_0 such that $L_z = 2\pi/(n\beta_0), n = 1, 2, \cdots$, while in aDNS L_z is a continuous free parameter. We discuss the two possibilities separately; in both cases we restrict the

discussion to simulations performed under initial and boundary conditions such that linear instability mechanisms alone can drive nonlinearity.

If a three-dimensional pDNS is performed at $Re = 950$ and a spanwise length of the integration domain L_z is chosen such that $\beta_0 > 8.3$, that is $L_z < 0.76$, neither β_0 nor any of the harmonics of this global linear eigenmode can be amplified. As a consequence one may predict, without performing the three-dimensional simulation, that the latter will converge in time to the same steady-state solution to which a two-dimensional $(\partial/\partial z \equiv 0)$ simulation converges. At the same Reynolds number value, a choice of spanwise wavelength $L_z \in [L_l, L_h] = [0.76, 0.95]$ will result in exponential amplification and, eventually, turbulent flow on account of the unstable fundamental wavenumber which is implicitly defined by a spanwise wavelength within this range. Finally, if $L_z > 0.95$ two distinct situations may be obtained; with the fundamental wavenumber being stable $(\beta_0 < 6.6)$, L_z may be taken such that none of its harmonics fit within the domain of unstable wavenumbers at this Reynolds number, or an L_z may be chosen such that some harmonic may be amplified. While in the first case the two-dimensional steady-state solution will be obtained, the result of a three-dimensional simulation in the second case will be transition to a turbulent flow state. The case of an aDNS may be perceived as a special case of a pDNS, since the homogeneous Dirichlet conditions imposed on the disturbance quantities are a subset of those admissible in a periodic simulation. Here there exist two possibilities, depending on whether L_z is smaller or larger than L_l. In the first case two- and three-dimensional simulations will deliver identical converged steady-state solutions while in the second, which includes the well-studied case of a cubic cavity, transition to turbulence should be expected on account of at least one three-dimensional $(\beta \neq 0)$ eigenmode having a wavenumber which fits into $\beta \in [6.6, 8.3]$ at this Reynolds number value.

At higher Reynolds number values the situation is qualitatively analogous for aDNS, with the dichotomy in wavenumbers being determined by the highest neutrally stable wavenumber value. For pDNS, on the other hand, the analogous discussion to that at $Re = 950$ applies at $L_z < L_l$ and $L_z \in [L_l, L_h]$. There exists a Reynolds number value, though, at which $\beta_h \geq 2\beta_l$; in such a situation, if $L_z > L_h$ there will always be some harmonic of β_0 which will correspond to an unstable mode having $\beta = n\beta_0 \in [\beta_l, \beta_h]$ which will be liable to linear amplification in the three-dimensional simulation and eventual departure of the three- from the two-dimensional numerical simulation results. The lid-driven cavity with its large body of numerical results is but one example of demonstration of this behaviour.

4. CONCLUSIONS

The questions which gave rise to the present work may be answered within the unifying framework of the reasonably novel global linear instability analysis of a two-dimensional steady solution of the equations of motion. Aided by the results of a numerically well-studied incompressible flow problem we were able to attach physical significance to the transient behaviour of two-dimensional time-dependent incompressible direct numerical simulation results. What is commonly known as residual in the simulation is either the least damped two-dimensional ($\beta = 0$)−linear eigenmode of the converged steady state itself, or can be related to a small number of the least damped modes of the full eigenvalue spectrum. As the Reynolds number increases, all global two-dimensional eigenmodes become increasingly less damped, until a parameter value is reached beyond which no steady-state solution exists. The physical information which is suppressed in two-dimensional simulations based on the steady formulation of the equations of motion concerns the dynamical behaviour of these two-dimensional linear eigenmodes. While unsteadiness should not be interpreted as amplification of the global linear ($\beta = 0$)−eigenmodes, on the simple

grounds of the absence of a converged steady-state upon which the latter would develop, the process leading to unsteadiness is directly linked with the diminishing magnitude of damping rates of the global linear modes as the flow Reynolds number increases, and the associated prevalence of nonlinearity.

When a steady-state solution exists, the insight gained from the association of the transient behaviour in two-dimensional DNS with the results of the nonparallel linear instability analysis of the converged steady-state may be used in a threefold manner. First, an algorithm may be constructed, to recover the steady-state solution from transient data taken well before convergence, thus making further time-integration of the equations of motion redundant. The algorithm, whose building elements were presented in §2.5, is based on identification of the parameters pertaining to the linear eigenmodes which determine the transient behaviour of the solution, namely the damping rate σ and the frequency ω_r of the least stable eigenmodes. Results shown in §3.5 on the example problem studied have demonstrated that up to three-quarters of the otherwise necessary computing effort may be saved by application of the theory of §2.5. Second, the results of a nonparallel linear instability analysis of the converged steady-state can be used as a quality test of the obtained solution, if the latter has been obtained using a time-accurate solution approach. The rate of decay of the residual which ultimately has to be damped in order for a converged steady-state to be obtained should equal the damping rate of the least-stable eigenmode, if both numbers are substantially larger than zero in magnitude. Disagreement of these two quantities indicates that the obtained steady-state still contains an unsteady component which must be eliminated by further time-integration, or by application of the ideas of §2.5. Third, the time necessary for the reduction of residuals to machine-roundoff level may also be estimated using nonparallel linear instability theory and is inversely proportional to the damping rate of the least damped linear eigenmode. Using the value of the damping rate

obtained by extrapolation of data at lower Reynolds numbers one predicts that in the square lid-driven cavity at $Re = 10^4$ a steady-state solution, if one exists, may be obtained after integrating the unsteady equations of motion for time in excess of $t = 4000$ as calculated from (7) and non-dimensionalised with the lid-velocity and the cavity length.

Well before the flow tends to lose its stability to two-dimensional linear eigenmodes, three-dimensional ($\beta \neq 0$)−disturbances may be amplified. Depending on the size of the observation window in the third spatial dimension, this amplification of three-dimensional global disturbances can explain the differences between the results of the two- and three-dimensional DNS. Again, caution is warranted at this point not to confuse amplification of the global, two-dimensional instabilities discussed here with solutions of the classic ordinary-differential-equation based eigenvalue problem, which are incorporated in those of (6a-6d); both mechanisms may provide amplification, as the laminar separation bubble flow example has clearly demonstrated [29]. Conversely, nonparallel linear instability theory provides a handle to probe into the physics of the flow in (three-dimensional) physical space using two-dimensional DNS results, before resorting to computationally intensive three-dimensional spatial DNS, at least as far as the response of the flow to small-amplitude excitations is concerned. Solution of the partial-derivative eigenvalue problem not only answers the question whether new physics is to be learnt by performing the three-dimensional DNS at a given set of parameters but also provides information on the physical mechanism which leads flow to deviate from two-dimensionality.

5. EPILOGUE

Based on the findings presented we may extend the discussion, in the form of proposed future work, to both one and three nonperiodic spatial directions. Both an one-dimensional and a three-dimensional steady-state solution $\bar{q}$ may be recovered by application of the ideas discussed herein for the case of two nonperiodic spatial directions. In the case of an

one-dimensional profile $\bar{q}$ being sought by time-marching the equations of motion, taking two spatial directions as periodic and resolving the third, the associated linear instability problem to be solved is based on the classic system of the one-dimensional Orr-Sommerfeld and Squire linear instability equations to which (6a-6d) reduce if the dependence of the basic flow on one of the two resolved spatial directions, say x, is neglected such that this spatial direction may be taken as homogeneous as far as the disturbance field is concerned. The linear mode associated with the residuals is the least stable member of the spectrum obtained at $\alpha = \beta = 0$, α and β being the wavenumbers along the periodic spatial directions, x and z. It is well appreciated in this case that agreement of the time-accurate simulation results and those of the one-dimensional linear instability problem is a minimum simulation quality criterion [12, 3]. However, given current hardware capabilities, it is likely that an one-dimensional $\bar{q}$ will be sought by a direct algorithm, rather than by time-marching the unsteady equations of motion. An extension of the algorithm presented for the recovery of a two-dimensional $\bar{q}$ is also possible in the case of flow developing in three nonperiodic spatial directions. In this case the existence of a steady-state $\bar{q}$ is synonymous with stability of all eigenmodes of the flow but current hardware technology makes the solution of the corresponding three-dimensional partial derivative eigenvalue problem impractical. On the other hand the ideas presented in § 2.5 may be used in order to recover a three-dimensional steady state once a regime of linear damping of residuals has been identified. The discussion presented may also be straightforwardly extended in compressible flow, in the absence of discontinuities. While two-dimensional numerical simulations for compressible flow in the presence of discontinuities are well advanced, the corresponding linear instability theory is only recently slowly emerging [32]. Both nonparallel linear instability theory in three nonperiodic spatial directions and that in the presence of discontinuities are worth pursuing in future studies.

REFERENCES

1. W. R. Briley. A numerical study of laminar separation bubbles using the Navier-Stokes equations. *J. Fluid Mech.*, 47:713–736, 1971.

2. O. R. Burggraf. Analytical and numerical studies of the structure of steady separated flows. *J. Fluid Mech.*, 24:113–151, 1966.

3. C. Canuto, M. Y. Hussaini, A. Quarteroni, and T. A. Zang. *Spectral methods in fluid dynamics.* Springer, 1987.

4. D. Barkley, G. Gomes, and R. D. Henderson. Three-dimensional instability in flow over a backward facing step. *J. Fluid. Mech*, (submitted), 1999.

5. Y. Ding and M. Kawahara. Linear stability of incompressible flow using a mixed finite element method. *J. Comput. Phys.*, 139:243–273, 1998.

6. P. G. Drazin and W. H. Reid. *Hydrodynamic Stability.* Cambridge University Press, 1981.

7. E. Leriche, S. Gavrilakis, and M. O. Deville. Direct numerical simulation of the lid-driven cavity flow with Chebyshev polynomials. In K. D. Papailiou, editor, *Fourth European Computational Fluid Dynamics Conference ECCOMAS'98*, pages 220–225, Chichester, N. York, 1998. J. Wiley and Sons.

8. H. C. Ku, R. S. Hirsch, and T. D. Taylor. A pseudospectral method for solution of the three-dimensional incompressible Navier-Stokes equations. *J. Comput. Phys.*, 70:549–462, 1987.

9. J. Kim and P. Moin. Application of a fractional-step method to incompressible Navier-Stokes equations. *J. Comput. Phys.*, 59:308–323, 1985.

10. J. Shen. Hopf bifurcation of the unsteady regularized driven cavity flow. *J. Comput. Phys.*, 95:228–245, 1991.

11. J. W. Goodrich, K. Gustafson, and K. Halasi. Hopf bifurcation in the driven cavity. *J. Comput. Phys.*, 90:219–261, 1990.

12. L. Kleiser and U. Schumann. Treatment of incompressibility and boundary conditions in 3-d numerical simulations of plane channel flows. In E. H. Hirschel, editor, *Proceedings, Third GAMM-Conference on numerical methods in fluid dynamics*, pages 165–173, Braunschweig, 1980.

13. L. L. Pauley, P. Moin, and W. C. Reynolds. The structure of two–dimensional separation. *J. Fluid Mech.*, 220:397–411, 1990.

14. M. Abramowitz and I. Stegun. *Handbook of mathematical functions.* Dover, 1970.

15. M. M. Rai and P. Moin. Direct simulations of turbulent flow using finite-difference schemes. *J. Comp. Phys.*, 96:15 – 33, 1991.

16. N. Y. Lee, W. W. Schultz, and J. P. Boyd. Stability of fluid in a rectangular enclosure by spectral method. *Int. J. Heat Mass Transfer*, 32:513–520, 1996.

17. P. R. Spalart, R. D. Moser, and M. M. Rogers. Spectral methods for the Navier-Stokes equations with one infinite and two periodic directions. *J. Comput. Phys.*, 96:297–324, 1991.

18. R. T. Pierrehumbert. A universal shortwave instability of two-dimensional eddies in an inviscid fluid. *Phys. Rev. Let.*, 57:2157–2159, 1986.

19. R. Schreiber and H. B. Keller. Driven cavity flows by efficient numerical techniques. *J. Comput. Phys.*, 49:310–433, 1983.

20. R. Schreiber and H. B. Keller. Spurious solutions in driven-cavity calculations. *J. Comput. Phys.*, 49:165–172, 1983.

21. N. Ramanan and G. M. Homsy. Linear stability of lid-driven cavity flow. *Phys. Fluids*, 6(8):2690–2701, 1994.

22. P. R. Spalart. Direct simulation of a turbulent boundary layer up to R_θ=1410. *J. Fluid Mech.*, 187:61 – 98, 1988.

23. V. Theofilis. Linear instability in two spatial dimensions. In K. D. Papailiou, editor, *Fourth European Computational Fluid Dynamics Conference ECCOMAS'98*, pages 547–552, Chichester, N. York, 1998. J. Wiley and Sons.

24. V. Theofilis. On linear and nonlinear instability of the incompressible swept attachment-line boundary layer. *J. Fluid Mech.*, 355:193–227, 1998.

25. W. Tollmien. Über die Entstehung der Turbulenz. *Nach. Ges. Wiss. Göttingen*, pages 21–44, 1929.

26. U. Ehrenstein and R. Peyret. A Chebyshev collocation method for the Navier-Stokes equations with application to double-diffusive convection. *Int. J. Num. Methods Fluids*, 9:427–452, 1989.

27. U. Ghia, K. N. Ghia, and C. T. Shin. High-Re solutions for incompressible flow using the Navier-Stokes equations and a multigrid method. *J. Comput. Phys.*, 48:387–411, 1982.

28. U. Rist and U. Maucher. Direct numerical simulation of 2–d and 3–d instability waves in a laminar separation bubble. In B. Cantwell, editor, *AGARD-CP-551 Application of Direct and Large Eddy Simulation to Transition and Turbulence*, pages 34–1 – 34–7, 1994.

29. V. Theofilis, S. Hein, and U. Ch. Dallmann. On the origins of unsteadiness and three-dimensionality in a laminar separation bubble. part i: Linear considerations. *Phil. Trans. Roy. Soc. (London) A*, (to appear), 1999.

30. W. E and J.-G. Liu. Essentially compact schemes for unsteady viscous incompressible flows. *J. Comput. Phys.*, 126:122–138, 1996.

31. W. E and J.-G. Liu. Vorticity boundary condition and related issues for finite-difference schemes. *J. Comput. Phys.*, 124:368–382, 1996.

32. X. Zhong. High-order finite-difference schemes for numerical simulation of hypersonic boundary-layer transition. *J. Comput. Phys.*, 144:662–709, 1998.

TABLE 1a

Location and value of the maxima of the primary and the lower-left (LL), lower-right (LR) and upper-left (UL) secondary vortices in the steady state solution for $\bar{\psi}$ and ζ at Re = 400, 1000, 3200 and 4000; comparisons with Ghia _et al._ [27] and Schreiber and Keller [19].

		$Re = 400$		
		Ghia _et al._ [27]	Schreiber and Keller [19]	present results
Primary	ψ	-0.1139	-0.1140	-0.1139
	ζ	2.29469	2.281	2.29584
	(x, y)	$(0.5547, 0.6055)$	$(0.5571, 0.6071)$	$(0.5535, 0.6054)$
LL	ψ	1.42×10^{-5}	1.45×10^{-5}	1.40×10^{-5}
	ζ	-0.0570	-0.0471	-0.05685
	(x, y)	$(0.0508, 0.0469)$	$(0.0500, 0.0429)$	$(0.0510, 0.0466)$
LR	ψ	6.42×10^{-4}	6.44×10^{-4}	6.41×10^{-4}
	ζ	-0.4335	-0.394	-0.44802
	(x, y)	$(0.8906, 0.1250)$	$(0.8857, 0.1143)$	$(0.8852, 0.1217)$

		$Re = 1000$		
		Ghia _et al._ [27]	Schreiber and Keller [19]	present results
Primary	ψ	-0.117929	-0.11603	-0.118902
	ζ	2.04968	2.02600	2.068251
	(x, y)	$(0.5313, 0.5625)$	$(0.52857, 0.56429)$	$(0.529654, 0.565018)$
LL	ψ	2.31×10^{-4}	2.17×10^{-3}	2.354097×10^{-4}
	ζ	-0.36175	-0.302	-0.337187
	(x, y)	$(0.0859, 0.0781)$	$(0.08571, 0.07143)$	$(0.081549, 0.077839)$
LR	ψ	1.75×10^{-3}	1.70×10^{-3}	1.744028×10^{-3}
	ζ	-1.15465	-0.999	-1.097921
	(x, y)	$(0.8594, 0.1094)$	$(0.86429, 0.10714)$	$(0.867381, 0.114469)$

		$Re = 3200$			
		Primary	UL	LL	LR
[27]	ψ	-0.12038	7.27682×10^{-4}	9.7823×10^{-4}	3.14×10^{-3}
	ζ	1.98860	-1.71161	-1.06301	-2.27365
	(x, y)	$(0.5165, 0.5469)$	$(0.0547, 0.8984)$	$(0.0859, 0.1094)$	$(0.81255, 0.0859)$
present	ψ	-0.12181	7.11201×10^{-4}	1.12331×10^{-3}	2.82648×10^{-3}
	ζ	1.961154	-1.65335	-1.16397	-2.24381
	(x, y)	$(0.51722, 0.54089)$	$(0.0524, 0.8981)$	$(0.08106, 0.12052)$	$(0.82281, 0.084648)$

		$Re = 4000$			
		Primary	UL	LL	LR
[19]	ψ	-0.11237		1.12×10^{-3}	2.80×10^{-3}
	ζ	1.805		-1.067	-2.145
	(x, y)	$(0.51875, 0.53750)$		$(0.08125, 0.11875)$	$(0.81875, 0.07500)$
present	ψ	-0.12203	1.073×10^{-3}	1.24736×10^{-3}	2.95426×10^{-3}
	ζ	1.94949	-1.91234	-1.27899	-2.42032
	(x, y)	$(0.51597, 0.53846)$	$(0.06098, 0.90387)$	$(0.08055, 0.12482)$	$(0.81640, 0.07983)$

TABLE 1b

Comparison of the interpolated values of our solutions on the maxima presented by Ghia *et al.* [27] and Schreiber & Keller [19]. An asterisk denotes Richardson-extrapolated data in the latter work.

	Primary		UL		LL		LR	
$Re = 400$	ψ	ζ	ψ	ζ	$10^5\psi$	ζ	$10^4\psi$	ζ
[27]	−0.113909	2.29469			1.41951	−0.05697	6.42352	−0.4335
present	−0.113989	2.29463			1.47210	−0.05711	6.42406	−0.4329
[19]	−0.11399*	2.2898*			1.45	−0.04710	6.440	−0.3940
present	−0.113982	2.29184			1.40	−0.04766	6.373	−0.4030

	Primary		UL		LL		LR	
$Re = 1000$	ψ	ζ	ψ	ζ	$10^4\psi$	ζ	$10^3\psi$	ζ
[27]	−0.117929	2.04968			2.31129	−0.36175	1.75102	−1.1547
present	−0.118902	2.06839			2.37806	−0.36575	1.77911	−1.1486
[19]	−0.11894*	2.0677*			2.1700	−0.302000	1.700	−0.9990
present	−0.118905	2.068234			2.3151	−0.312162	1.763	−1.0481

	Primary		UL		LL		LR	
$Re = 3200$	ψ	ζ	$10^4\psi$	ζ	$10^3\psi$	ζ	$10^3\psi$	ζ
[27]	−0.120377	1.9886	7.27	−1.71161	0.98	−1.06301	3.14	−2.27365
present	−0.121777	1.9612	7.08	−1.73137	1.09	−1.00607	2.77	−2.25511

	Primary		UL		LL		LR	
$Re = 4000$	ψ	ζ	ψ	ζ	$10^3\psi$	ζ	$10^3\psi$	ζ
[19]	−0.12202*	1.9498*			1.1200	−1.0670	2.8000	−2.14500
present	−0.122026	1.94960			1.2411	−1.1427	2.9228	−2.31944

TABLE 2

Comparison of the least stable eigenmode at $Re = 200$ against the results of Ramanan and Homsy [21] (RH) and the graphically (digitally) reproduced growth rate result of Ding and Kawahara [5] (DK).

β	RH		DK	present results	
	ω_r	ω_i	ω_i	ω_r	ω_i
1	±0.00	−0.34	−0.3183	±0.0000	−0.3297
2	±0.00	−0.23	−0.2248	±0.0000	−0.2267
3	±0.11	−0.29	−0.2924	±0.1073	−0.2954
4	±0.28	−0.30	−0.2969	±0.2810	−0.2956
5	±0.43	−0.34	−0.3431	±0.4260	−0.3404
6	±0.58	−0.39	−0.3893	±0.5821	−0.3844
7	±0.67	−0.41	−0.4073	±0.6733	−0.4013
8	±0.72	−0.45	−0.4637	±0.7232	−0.4587
9	±0.76	−0.54	−0.5504	±0.7622	−0.5473

TABLE 3

Numerical results for the rate of decay of residuals σ as a function of resolution at different low Reynolds numbers. Also shown the result of numerical solution of (6a-6d) for the imaginary part of the eigenvalue ω_i, using the respective converged steady-state as basic flow.

| | *Re* | | |
Resolution	100 σ	200 σ	300 σ
16×16	-0.5404	-0.3248	-0.2865
24×24	-0.5407	-0.3319	-0.2843
32×32	-0.5409	-0.3318	-0.2842
40×40	-0.5409	-0.3318	-0.2842
ω_i	-0.5410	-0.3319	-0.2845

TABLE 4

Numerical results for the damping rate ω_i of the least stable $(\beta = 0)$–eigenmode at $Re = 2500, 5000$ and 7500 and its discrepancy in percentage terms from the rate of decay of residuals σ.

Re	ω_i	$\frac{|\omega_i - \sigma|}{|\sigma|} \times 100$
2500	-0.0253	1.2
5000	-0.0112	8.9
7500	-0.0093	17.8

TABLE 5

Contour levels for the spatial structure of the normalised eigenfunctions pertaining to the least stable global $(\beta = 0-)$eigenmode at $Re = 1000$, whose eigenvalue is $\omega = (0.0, -0.068)$; $x(y) \equiv x \times 10^y$.

$\hat{u}$ level	symbol	$\hat{v}$ level	symbol	$\hat{w}$ level	symbol	$\hat{p}$ level	symbol
$+/-9(-1)$	A / a	$+/-9(-1)$	A / a	.9	a	.90	a
$+/-6(-1)$	B / b	$+/-6(-1)$	B / b	.7	b	.80	b
$+/-3(-1)$	C / c	$+/-3(-1)$	C / c	.5	c	.70	c
$+/-6(-2)$	D / d	$+/-6(-2)$	D / d	.3	d	.60	d
$+/-2(-2)$	E / e	$+/-2(-2)$	E / e	$+/-.1$	e / g	.45	e
$+/-1(-3)$	F / f	$+/-1(-3)$	F / f	0	f	.30	f
				$-.2$	h	.15	g
						0	h
						$-.15$	i
						$-.20$	j

TABLE 6

Recovery of $\bar{\psi}$ from transient data at $Re = 100, 400$ and 1000 as function of resolution and time-step used in the DNS. $x(y) \equiv x \times 10^y$.

	$Re = 100$		
Resolution	16×16	24×24	32×32
Δt	0.01	0.01	0.005
$\bar{t}$	50.43	50.42	49.005
$\tilde{t}$	12.71	12.79	11.07
$-\sigma$	0.540246	0.540214	0.540876
$\max(\Delta\tilde{\psi})$	5.3(−8)	8.8(−7)	4.6(−6)
$\min(\Delta\tilde{\psi})$	3.6(−9)	7.9(−8)	5.1(−7)
$\max(\Delta\psi)$	3.4(−4)	3.5(−4)	1.0(−3)
$\min(\Delta\psi)$	1.5(−5)	1.2(−3)	1.6(−2)

	$Re = 400$		
Resolution	16×16	24×24	32×32
Δt	0.01	0.01	0.01
$\bar{t}$	117.82	110.91	110.27
$\tilde{t}$	26.43	23.43	23.43
$-\sigma$	0.267091	0.258176	0.258280
$\max(\Delta\tilde{\psi})$	5.2(−5)	3.6(−5)	1.3(−5)
$\min(\Delta\tilde{\psi})$	7.0(−6)	1.9(−5)	7.7(−6)
$\max(\Delta\psi)$	2.8(−3)	1.2(−2)	9.5(−3)
$\min(\Delta\psi)$	8.0(−4)	2.1(−3)	2.4(−3)

	$Re = 1000$		
Resolution	24×24	32×32	40×40
Δt	0.01	0.01	0.01
$\bar{t}$	325.93	323.61	324.33
$\tilde{t}$	77.82	77.53	77.81
$-\sigma$	0.065808	0.065657	0.065336
$\max(\Delta\tilde{\psi})$	2.9(−6)	9.5(−5)	3.1(−5)
$\min(\Delta\tilde{\psi})$	4.9(−7)	3.2(−6)	3.3(−6)
$\max(\Delta\psi)$	3.7(−4)	3.6(−4)	2.5(−4)
$\min(\Delta\psi)$	3.7(−4)	5.1(−4)	3.3(−4)

TABLE 7

Recovery of $\bar{q}$ at several Reynolds numbers from transient data at times beyond that at which ω converges. The discrepancy between σ and ω_i of the least stable eigenmode is also presented. $Re = 100$ and 400 runs on a 32^2 grid; $Re = 1000$ run on a 40^2 grid. $x(y) \equiv x \times 10^y$.

$\frac{t}{\tilde{t}} \times 100$	$\max(\Delta\psi)$	$\min(\Delta\psi)$	$\frac{|\sigma - \omega_i|}{|\omega_i|} \times 100$
		$Re = 100$	
22.59	4.6(−6)	5.1(−7)	0.023
25.02	4.0(−8)	1.9(−8)	0.018
30.90	2.5(−9)	1.2(−9)	0.011
35.12	1.8(−10)	1.0(−10)	0.009
		$Re = 400$	
21.25	1.3(−5)	7.7(−6)	19.10 / 11.71 / 6.85
25.03	8.4(−6)	3.5(−6)	18.88 / 11.49 / 7.07
30.05	2.6(−6)	9.5(−7)	18.26 / 10.88 / 7.67
35.61	1.3(−6)	5.6(−7)	18.04 / 10.66 / 7.90
		$Re = 1000$	
23.99	3.1(−5)	3.3(−6)	3.97
25.02	1.3(−5)	1.5(−6)	3.35
30.23	2.1(−6)	1.2(−7)	0.65
35.02	1.5(−8)	5.8(−9)	0.24
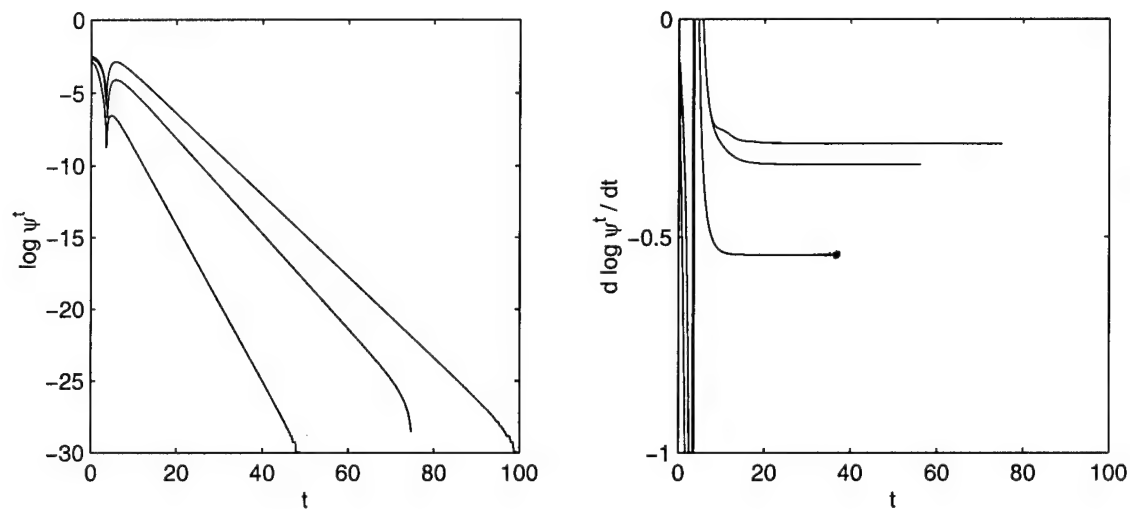
FIG. 1. Convergence history of stream function $\psi(0.5, 0.5)$ against time (left) and slope of this curve (right). Lower to upper curves, $Re = 100, 200$ and 300, respectively.
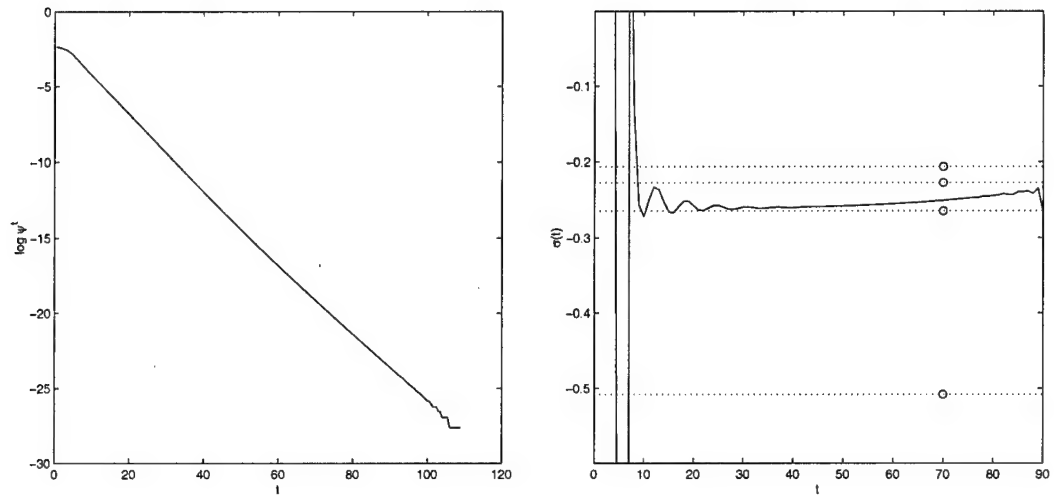
FIG. 2. Convergence history of $\psi(0.5, 0.5)$ against time at $Re = 400$ (left) and its slope (right). Superimposed and denoted by symbols are the eigenvalues of the four least stable global flow eigenmodes.
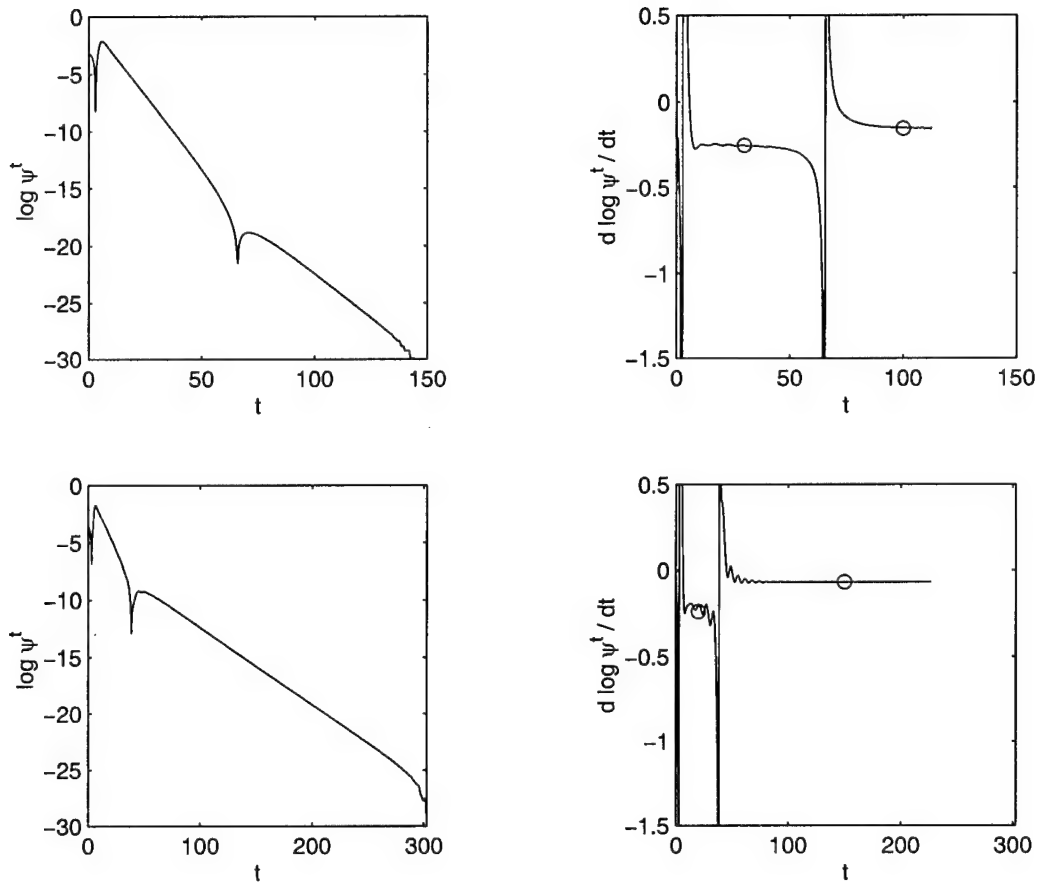
FIG. 3. Convergence history of $\psi(0.5, 0.5)$ against time at $Re = 500$ (upper left) and its slope (upper right); lower left and right, respectively, the corresponding results at $Re = 1000$. In both cases superimposed and denoted by symbols are the eigenvalues of the two least stable stationary modes.
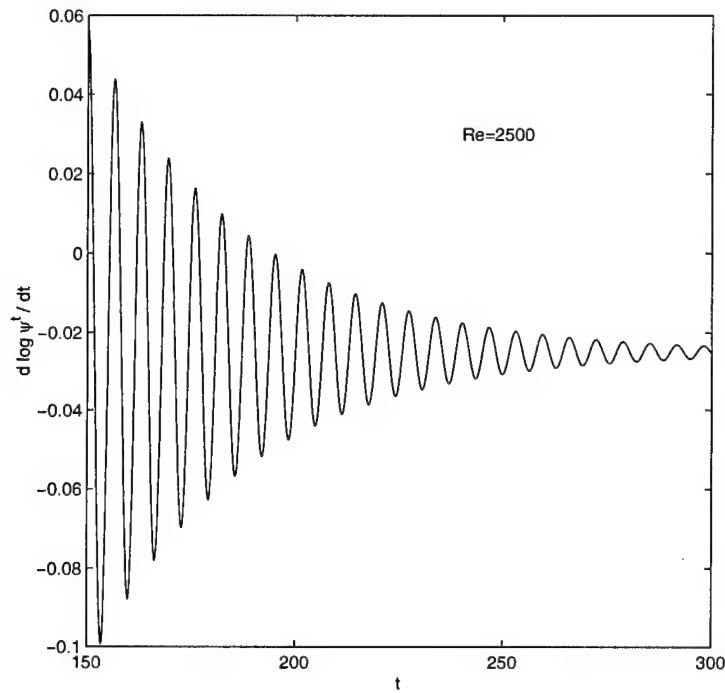
FIG. 4a. The dependence of the function $d(\ln \psi^t)/dt$ on time t, showing the exponential decay of a single travelling mode $(\omega_r \approx 0.97 \pm 0.01)$ superimposed upon the least damped exponentially decaying stationary disturbance at $Re = 2500$.
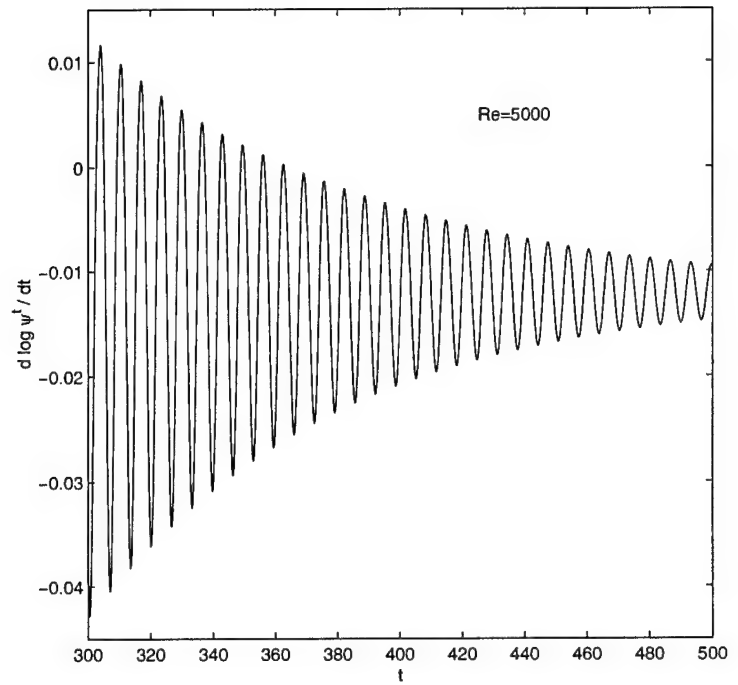
FIG. 4b. $Re = 5000$
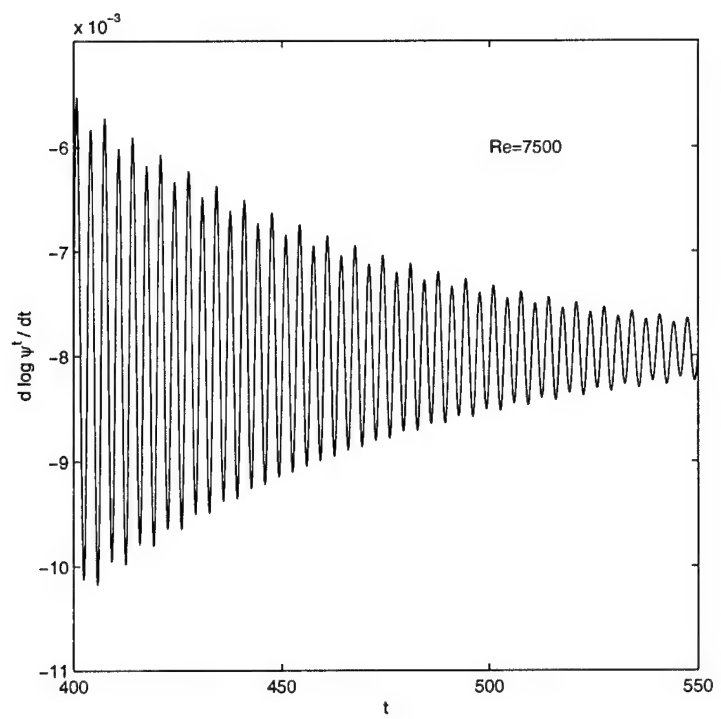
FIG. 4c. $Re = 7500$
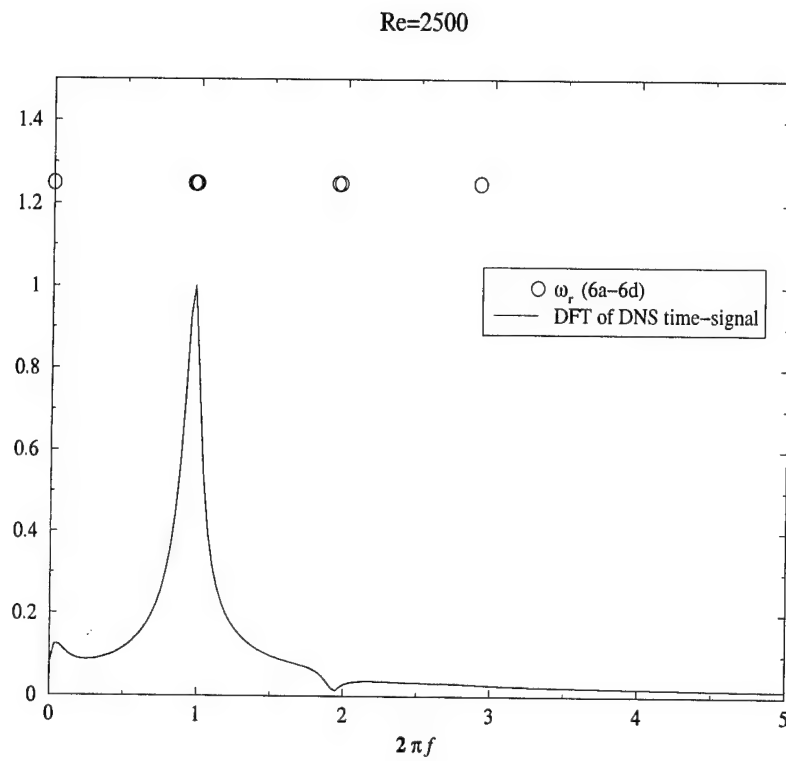
Re=2500

FIG. 5a. The correspondence of the frequencies of the damped linear $(\beta = 0)$ two-dimensional eigenmodes of the converged steady-states at different Reynolds numbers and those obtained from discrete Fourier transforms of the DNS signals. $Re = 2500$.

Re=5000
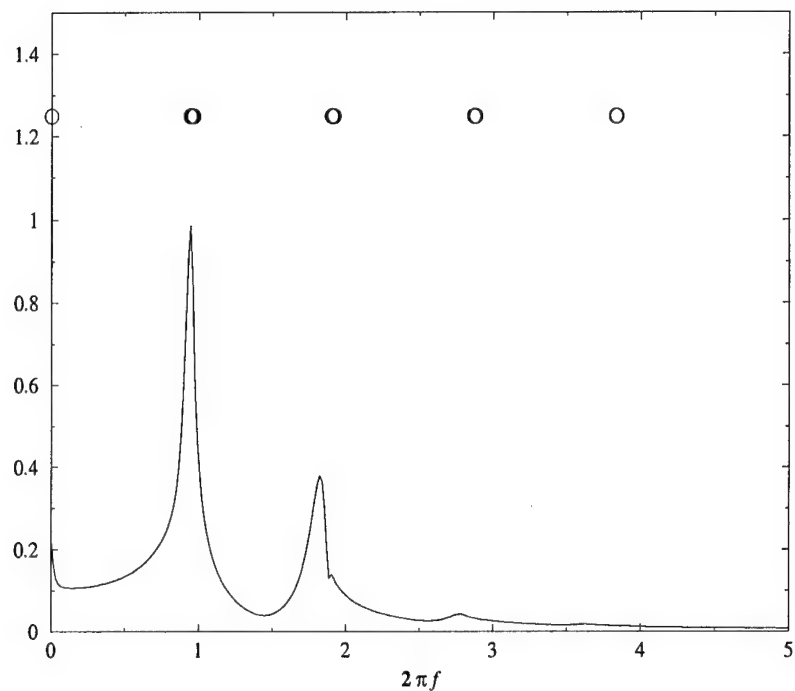
FIG. 5b. $Re = 5000$

Re=7500
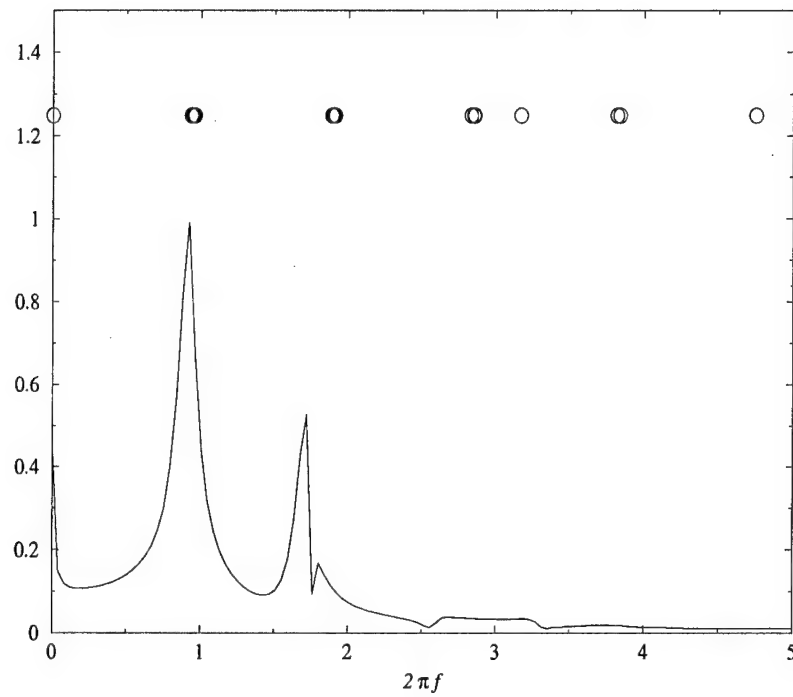
FIG. 5c. $Re = 7500$
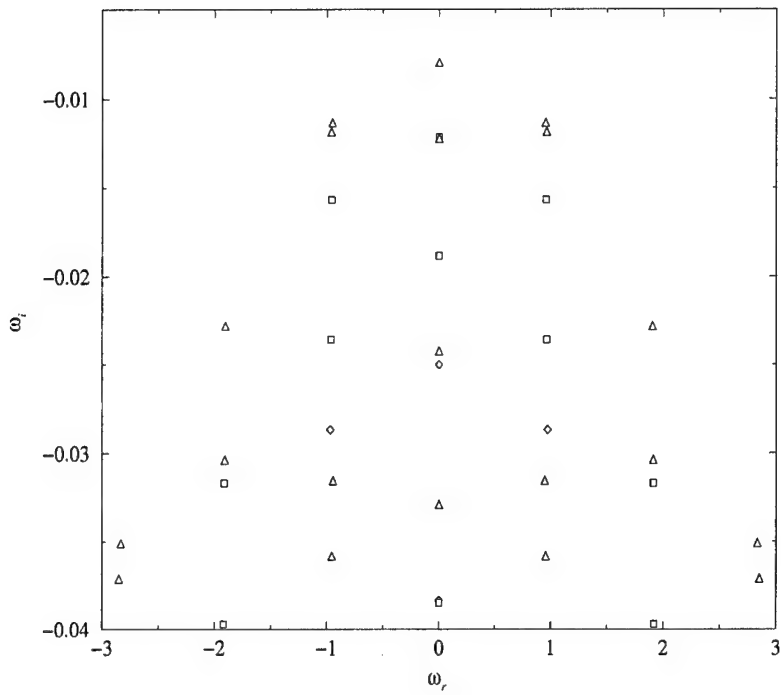
FIG. 6. The filling up of the eigenvalue spectrum as Reynolds number increases; $Re = 2500$ (diamond), **5000** (square), and **7500** (triangle).
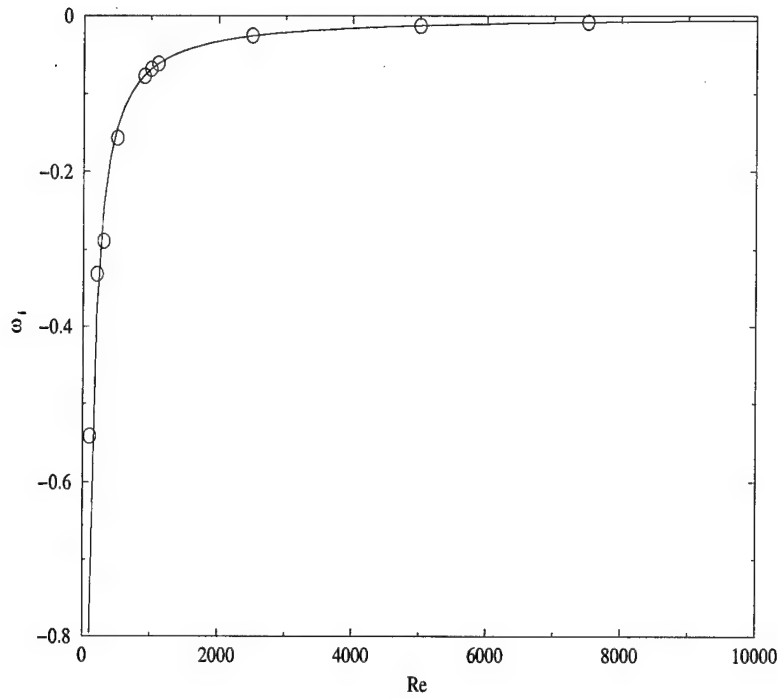
FIG. 7. The dependence of the damping rate ω_i of the least damped two-dimensional eigenmode of the converged steady-state at a Reynolds number on Re as predicted by the model (18) denoted by the solid line, and as calculated by numerical solution of the eigenvalue problem (6a-6d) denoted by the symbols.
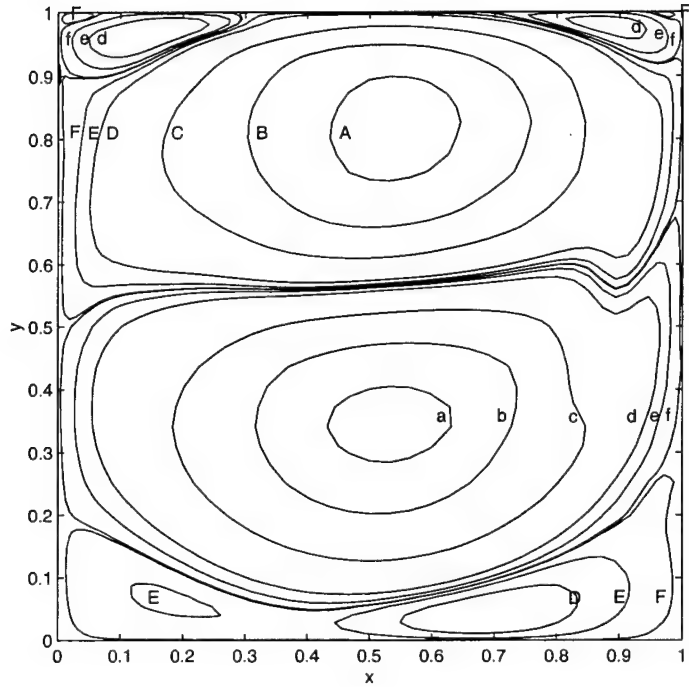
FIG. 8. Spatial distribution of the disturbance eigenvector of the least damped global linear eigenmode at $Re = 1000$: Disturbance velocity component $\hat{u}$.
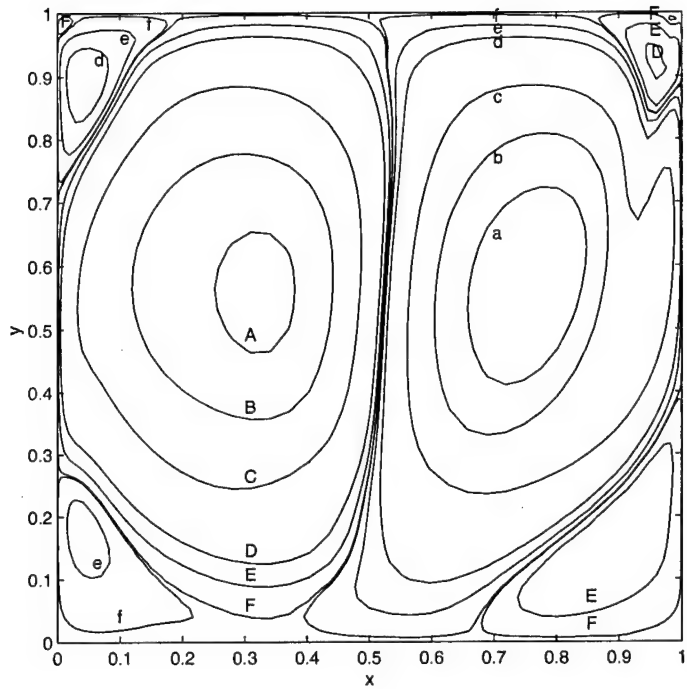
FIG. 8—*Continued*
Disturbance velocity component $\hat{v}$.
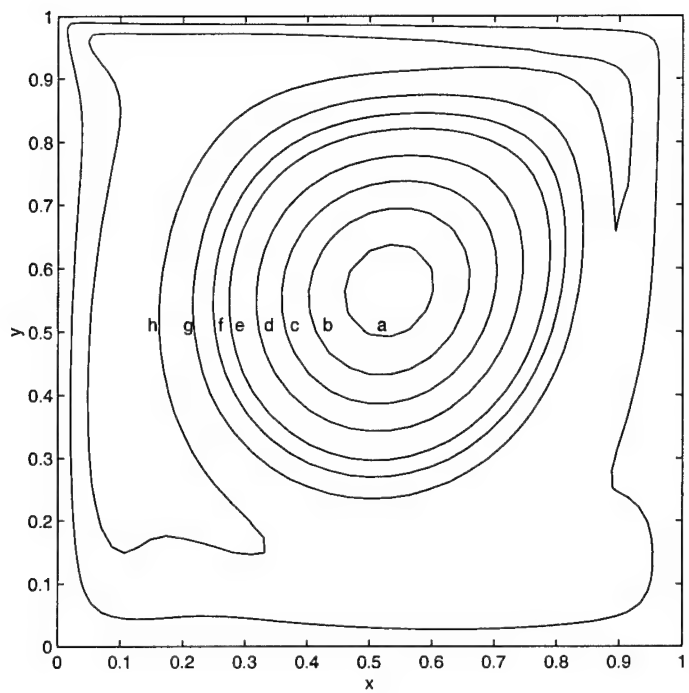
FIG. 8—*Continued*

Disturbance velocity component $\hat{w}$.
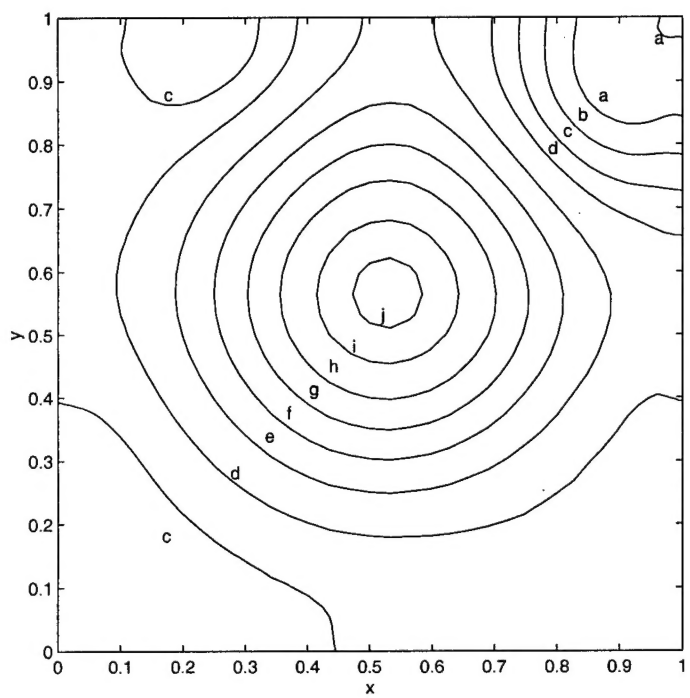
**FIG. 8**—*Continued*
Disturbance pressure $\hat{p}$.
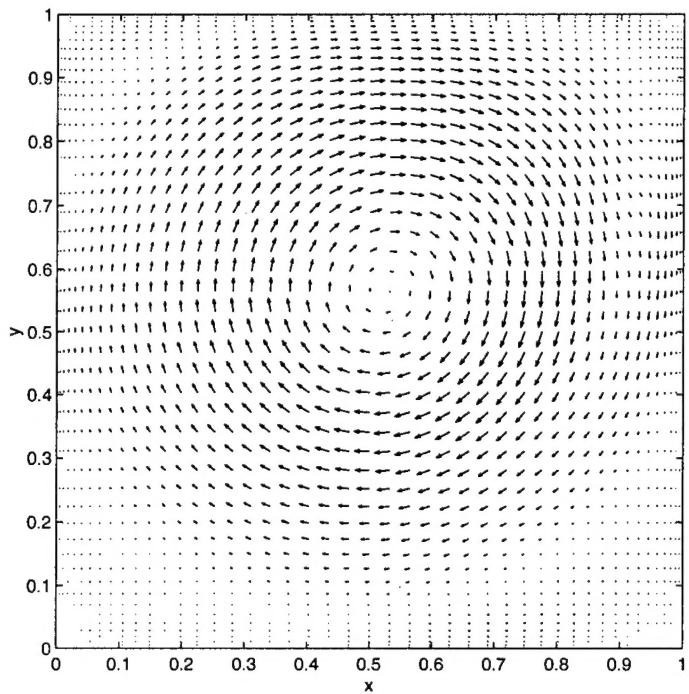
**FIG. 9.** Flowfield set up by combination of $\hat{u}$ and $\hat{v}$.
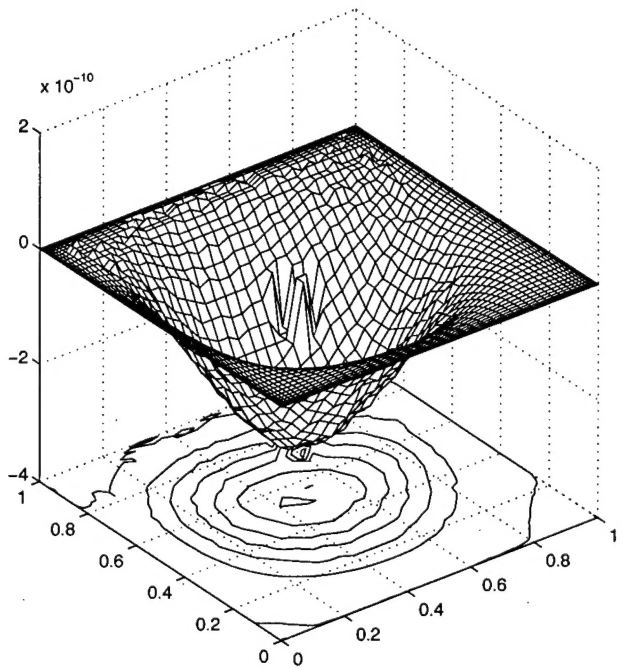
FIG. 10. The spatial distribution of the difference $\Delta\tilde{\psi}(x, y) \equiv \tilde{\psi} - \bar{\psi}$ at $Re = 100$ using $Nx = Ny = 48$ Jacobi collocation points.
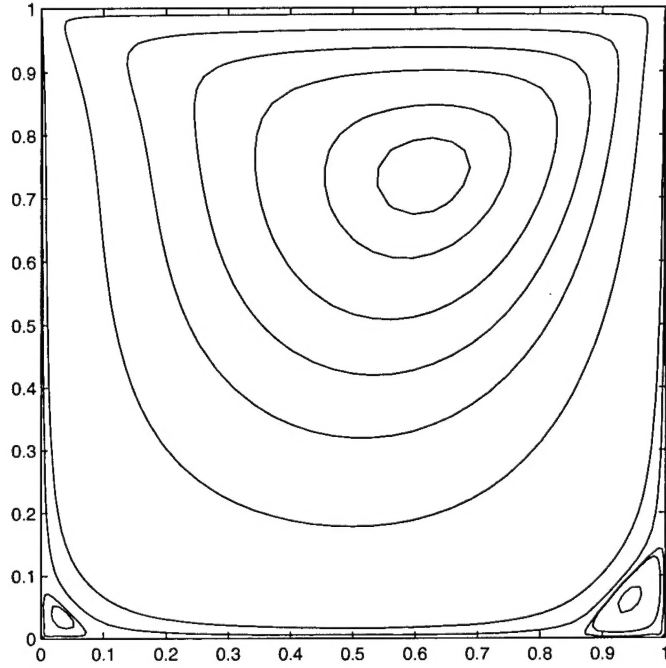
FIG. 11. An estimate of the converged solution $\tilde{\psi}$ at $Re = 100$ obtained by evaluating (12) at $t = 15$ and using $Nx = Ny = 48$ Jacobi collocation points. Iso-contours are drawn at the levels shown by Ghia *et al.* [27]